R. & M. No. 3151
(15,023)
A.R.C. Technical Report

MINISTRY OF AVIATION

AERONAUTICAL RESEARCH COUNCIL
REPORTS AND MEMORANDA

The Effect of Diameter Ratio on the Performance of a Low-Stagger Axial-Compressor Stage

By

R. A. JEFFS and R. G. ADAMS

LONDON: HER MAJESTY'S STATIONERY OFFICE
1960
PRICE 10*s.* 6*d.* NET

The Effect of Diameter Ratio on the Performance of a Low-Stagger Axial-Compressor Stage

By

R. A. Jeffs and R. G. Adams

Reports and Memoranda No. 3151*

April, 1952

Summary.—Low-speed tests have been carried out on a family of three single-stage compressors of different diameter ratios. The simple blade design tested showed considerable variations of performance as the diameter ratio was decreased from 0·65 to 0·35 but most of these variations are predictable by simple means and it is expected that they may be partially avoided by appropriate design methods.

It is recommended that low-stagger constant α_3 stages of low diameter ratio should be designed on the basis of radial equilibrium after the inlet guide blades. In the interests of minimizing the loss of working range at low diameter ratios, at least the outer half of the blades should be designed as far below nominal conditions as other considerations allow. The performance of such stages is fairly well estimated by integration of the strip performances of the various sections of the blade, though further information is necessary to fully define the work-done characteristic.

Evidence is shown that the establishment of radial equilibrium demands an axial distance which increases considerably with decreasing diameter ratio, and it is suggested that conditions upstream of a stator-blade row are influenced by conditions required for radial equilibrium downstream of that row.

1. *Introduction.*—In the application of the gas turbine to the high-speed-aircraft field, where the overall diameter of the engine becomes of great importance, designers are continually tempted to increase the air mass flow per unit frontal area of the engine by decreasing the hub diameter of the axial compressor for a given tip diameter, until the limiting factors become mechanical rather than aerodynamic. The information available relating to axial-compressor stages with low values of the ratio of hub diameter to tip diameter or ' diameter ratio ' is, however, exceedingly small, particularly on general design problems such as the significance of radial equilibrium, and methods of predicting the performance characteristics of such stages, where the individual section characteristics may be expected to be widely different at root and tip of the blades.

A series of tests was therefore planned which would provide some evidence on these lines, and indicate the aerodynamic penalties which may have to be paid for the use of these low diameter ratios. This series of tests compared the performance of three single-stage compressors with aerodynamically similar blading but having different diameter ratios, namely, 0·65, 0·5 and 0·35. Of these, the 0·65 ratio was essentially a conventional datum for comparison purposes, the 0·5-ratio stage represented the limit of present experience, while the 0·35 stage was expected to show up in more drastic fashion any difficulties and problems involved.

Since an important requirement of the tests was that the results be quickly available, a rig was evolved which was relatively simple and therefore easily, quickly and cheaply manufactured with a life sufficient for a specific series of tests.

* National Gas Turbine Establishment report R.117, received 23rd June, 1952.

These first tests have been carried out on a very simple low-stagger design of blading, in which no attempt has been made to use special methods of design for the low-diameter-ratio stages. It was expected that this would prove the most instructive way of learning the best method of design.

2. *Test Equipment.*—The rig consists of a single-stage compressor, with its associated motor and ducting.

The prime requirement of the rig was that overall stage characteristics and detailed observations of the airflow pattern could be simply taken. The second important point considered was the rapid manufacture required of both the rig and also the blading. This has been satisfied by extensive use of wood in the construction of the rig, metal-work being reduced to a minimum. By restricting the rotational speed of the rig to 1,500 r.p.m. and below, it has been possible to make the blades of low-melting-point alloys cast into wooden moulds.

The rig designed and built is illustrated in Fig. 1.

2.1. *The Compressor Test Rig.*—In order to keep to a minimum the number of new parts necessary for successive compressors, the outside diameter of the flow annulus has been kept constant, the diameter ratio being changed by alteration of the inside diameter. Thus the stator casing which carries a large part of the instrumentation has a diameter of 20 in. and three separate rotor assemblies of 7-in., 10-in. and 13-in. diameter have been made to fit into it. An alteration of diameter ratio simply involves the removal of one hub assembly, including inside-diameter inlet fairing, bladed rotor disc and diffuser bullet, reblading and reassembly with the hub parts of the appropriate diameter. The range of diameter ratio investigated is shown in Fig. 2.

The compressors are driven directly by a variable-speed electric motor and discharge air through a ducting system which has been designed to give as efficient and stable a diffusion as possible in order that the maximum amount of the characteristic may be measured. This ducting consists of a parallel section five blade chords long, an annular diffuser of constant outer diameter with a 7-deg conical bullet, a plain diffuser of 7 deg cone angle giving a final diameter of 30 in. and an adjustable annular throttle.

The tip clearance in each of the three compressors was kept at approximately 1 per cent of the blade height.

2.2. *Instrumentation.*—The various quantities involved in testing the compressors were measured by the following means :

(*a*) *Mass flow.*—This was measured when the compressor was running in a stable condition by a ring of four static-pressure tappings on the stator casing 0·4 blade chords upstream of the inlet guide blades, the reading given by a manifold linking the four tappings having been calibrated by pitot, yaw angle and static-pressure traverses across the annulus, in one circumferential position near the top centre, in the same plane as the tappings.

This method of calibration, though apparently rather superficial, is likely to be consistently in error for the three compressors. The absolute error will not invalidate the conclusions drawn, since these are based primarily on a comparison of the various experimental data.

(*b*) *Temperature rise.*—Since the temperature rise through the stage was less than 0·5 deg C no attempt at direct measurement of this quantity was made. It was computed from the mass flow and input power, and for this purpose, the driving motor was swung for torque-reaction measurement. The motor used, however, was rather heavy for its output power, being an A.C. commutator type of machine, which would have meant that a considerable percentage inaccuracy would have been inherent in any ball or roller trunnion mounting. This conventional method of mounting was therefore avoided, and the trunnion bearings in which the motor is swung are airborne, resulting in negligible trunnion friction. These bearings were designed on the basis of Shires's results[1] and have proved very satisfactory. The torque reaction being small, it was

found possible to measure it by means of a direct weigh-beam mounted on the motor with no mechanical linkage or pivots. It consists simply of a calibrated weight moving on an accurate lead screw.

The temperature at inlet to the compressor was measured by mercury-in-glass thermometers.

(*c*) *Rotational speed.*—Mounted on the motor end casing is an aircraft-type engine-speed generator which gives an approximate indication of the compressor rotational speed. A Hasler tachometer is used for more accurate measurement, and is accommodated by a slight modification to the back of the engine-speed generator which enabled the Hasler to be used on the generator shaft.

Good speed control was obtained ($\pm$ 2 r.p.m.) provided a range of approximately $\pm$ 100 r.p.m. near to the synchronous speed was avoided, in which considerable 'hunting' occurred.

(*d*) *Pressure rise.*—The overall total pressure rise through the compressor was measured by four combs of pitot-tubes spaced equally round the annulus, at 2·5 blade chords downstream of the trailing edge of the stator blades. Each comb consisted of seven tubes spaced across the annulus in such a way as to give a good picture of the flow distribution and twisted to point in the direction of the design air angles. The mean total pressure was obtained by integration of the readings of manifolds linking corresponding tubes in each comb.

On the 0·65-diameter-ratio compressor, the mean total head over one blade pitch after the inlet guide blades and after the stator blades was measured by means of a comb of nine pitot-tubes which was traversed circumferentially. This enabled the total pressure rise across the stage to be measured independent of any extraneous losses.

Static-pressure tappings were provided on the outer diameter of the annulus before the inlet guide blades, at 0·4 chords downstream of every blade row, and on outer and inner diameters in the plane of the pitot combs.

(*e*) *Detailed flow analysis.*—Closer examination of the airflow between the blade rows was made possible by the provision of a traversing gear which was capable of yawing instruments and traversing them radially. This could be mounted on slides which covered circumferential slots in the stator casing. Axial spacing of 0·8 $\times$ mean blade chord allowed insertion of instruments between the blade rows. It was thus possible to examine the flow over two blade pitches after every blade row. Radial traversing only at a position near the top centre was possible upstream of the inlet guide row.

The traversing instruments used were a normal type arrow-head pitot yaw-meter made of 1·5-mm hypodermic tubing and a 1-mm diameter static tube.

2.3. *Blading Design.*—As remarked previously, the first series of tests have been carried out on a very simple blade design, in which no attempt was made to anticipate any troubles which may arise with low diameter ratios. The design specifications were :

(*a*) Work done, ΔT, constant at all radii

(*b*) Axial velocity, V_a, constant at all radii

(*c*) Stator air inlet angle, α_3, constant at all radii

(*d*) Blade chord, c, constant at all radii

(*e*) 50 per cent reaction at mean radius

(*f*) Pitch/chord ratio, s/c, at mean radius = 0·9

(*g*) Blade speed/axial velocity, U/V_a, at mean radius = 1·25

(*h*) Deflection at mean radius given by

$$\tan \alpha_1 - \tan \alpha_2 = \frac{1 \cdot 55}{1 + 1 \cdot 5 s/c} \qquad \text{(Ref. 2).}$$

These assumptions are sufficient to specify the air angles. From these the blade angles were obtained by the methods of Refs. 3 and 4, so that at the design point, all blade sections should operate at nominal incidence. Full details are given in Appendix I and Fig. 3.

The blades were made as noted earlier by casting low-melting-point alloys into wooden moulds. The metals used initially were Fry's No. 2 alloy (Wood's metal) for the stator blades, with an ultimate strength of 1·6 tons per sq in. and Fry's No. 11 alloy for the rotor blades, with a strength of 3·9 tons/sq in. Later, the use of Wood's metal was abandoned because of trouble due to loss of strength with relatively high summer atmospheric temperatures.

2.4. *Test Technique.*—It was intended that all the compressors should be tested at the same mean radius Reynolds number based on conditions at inlet to the rotor. The 0·35 and 0·5-diameter-ratio compressors were tested at rotational speeds of 1,330 r.p.m. and 1,200 r.p.m. respectively, corresponding to a Reynolds number of $0{\cdot}9 \times 10^5$. Unfortunately, the 0·65-diameter-ratio stage had to be tested at a somewhat higher speed than that which would have given the same Reynolds number, because of instability of the motor speed near its synchronous speed, and this stage was therefore tested at a Reynolds number of $1{\cdot}04 \times 10^5$.

No tests have been carried out to investigate the variation of overall performance of these stages with Reynolds number, but tests on the variation of air outlet angle from the stator blades, together with previous experience on these effects[5], suggest that these tests were carried out in a region clear of the worst effect of this parameter. It is expected therefore that the overall performances measured on these tests are comparable with each other without correction for Reynolds number, though it is probable that the efficiencies are some 2 per cent lower than would be expected nearer ' full-scale ' Reynolds number.

Overall characteristics of temperature rise, pressure rise and efficiency were measured at these speeds. The pressure rise and efficiency were based on both static and total pressure rises, measured as explained in Section 2.2. (*d*).

Inter-row traverses of total and static pressure and yaw angle were also carried out. On the 0·35 and 0·5 compressors, preliminary circumferential traverses showed that the axial velocity distributions could be measured with good accuracy by radial traverses in a circumferential position clear of the blade wakes and this method was therefore adopted.

3. *Test Results.—Overall Characteristics.*—3.1. *General.*—The overall characteristics plotted non-dimensionally as temperature-rise coefficient, $Kp\Delta T/\frac{1}{2}U_m^2$, pressure-rise coefficient $\Delta p/(\frac{1}{2}\rho U_m^2)$ and isentropic efficiency, η_{is}, against mass-flow coefficient, $\bar{V}_a/U_m$, are plotted in Figs. 4 and 5. The pressure and efficiency are based on the static-pressure rise on the outer diameter of the flow annulus from after the inlet guide blades to after the stator blades.

The important observations from these curves are that, as the diameter ratio was decreased from 0·65 to 0·35,

(*a*) the work done at the design flow-coefficient of 0·8 increased

(*b*) the arithmetic slope of the temperature-rise characteristic increased

(*c*) the maximum efficiency and optimum flow increased

(*d*) the working range decreased.

A comparison has been made between these characteristics and those predicted by normal methods, which are based primarily on the mean diameter cascades. Plotted in Figs. 6 and 7 are the characteristics calculated by the general methods of Ref. 6 using the cascade data of Ref. 3. Special allowance has not been made for the somewhat lower losses associated with secondary flows and induced drag which may well occur with single stages of low diameter ratios, and the only differences in the characteristics for the different diameter ratios are due to the varying importance of the annulus drag. No work-done factor has been applied to the calculations, though a figure of 0·98 is frequently used for a first stage.

3.2. *Temperature Rise.*—The simple theoretical calculation allows no alteration in work done at design flow with change of diameter ratio. By comparison, the experimental characteristics show work-done factors of 1·03, 1·025 and 1·0 for diameter ratios 0·35, 0·5 and 0·65 respectively. Also, the slope of the theoretical curve is independent of diameter ratio and is considerably higher than any of the experimental curves.

The agreement with the predicted design-point work done is, therefore, reasonable at high diameter ratio, but falls off as the diameter ratio is decreased. The second phenomenon, about the slope of the characteristic, has been observed by Carter[7] on full-scale compressors, and will be discussed in more detail later.

3.3. *Pressure Rise and Efficiency.*—It is significant that although the standard calculation predicts an increase of efficiency with decreasing diameter ratio, it does not indicate the very high values of optimum flow shown by the experimental curves especially at low diameter ratios. The only theoretical characteristics which approach the form of the experimental curves are those corresponding to the ' strip ' performance of the tip section of the blades, calculated by a method to be described in Section 5. These characteristics are plotted in Fig. 7 and both the shapes of the curves and the trends of the values are remarkably similar to the experimental ones. This suggests that the static-pressure rise, on which the experimental characteristics were based, may be largely influenced by the tip-section performance, when this differs from the mean-stage performance.

These two need be identical only when the various factors influencing the static-pressure distribution combine to give the same static-pressure rise at all radii. Of these factors, the variation of work done up the blade height, especially at the low-mass-flow end of the characteristic, certainly does not suggest uniform static-pressure rise, while the modification of the static-pressure gradient during the establishment of radial equilibrium is uncertain without considerable further work on the rate at which equilibrium is set up. It appears, therefore, that any coincidence between the outside-diameter static-pressure rise and a mean-stage pressure rise is largely fortuitous, and the discrepancy between them may be expected to vary with the stage design, including the diameter ratio.

In the design of the rig, provision was made for measurement of the total pressure rise by means of 4 pitot combs, of 7 tubes each, spaced round the annulus about 2·5 blade chords downstream of the stator blades. Unfortunately the pressure rise thus recorded includes the losses in the compressor intake and the inlet guide blades, and also any loss associated with the change of velocity distribution downstream of the stator blades. The total-pressure characteristics for the 0·35 and 0·5-diameter-ratio stages have been calculated and corrected as far as possible for the experimentally determined inlet losses. The mixing loss behind the stator has not been allowed for because of scarcity of information, but the error is likely to be small. The characteristics for the 0·65-diameter-ratio stage were measured directly, as previously explained.

These characteristics are presented in two ways : by radial mean integration across the annulus, and by mass mean integration, where these are defined as :

$$\text{Radial mean pressure} = \frac{1}{(r_2 - r_1)} \int_{r_1}^{r_2} P \, dr$$

$$\text{Mass mean pressure} = \frac{2}{(r_2^2 - r_1^2)} \int_{r_1}^{r_2} r \frac{V_a}{\bar{V}_a} P \, dr .$$

A further definition, the annulus area mean, where

$$\text{annulus area mean pressure} = \frac{2}{(r_2^2 - r_1^2)} \int_{r_1}^{r_2} r \, P \, dr$$

has not been evaluated, but would probably come between the other two. Of these various definitions of mean pressure, it is considered that the ' mass mean ' value gives the truest picture of the total pressure energy in the air stream, and compares directly with the mean temperature rise computed as in these tests from total mass flow and input power.

These experimental total-pressure characteristics are plotted with the associated efficiencies in Figs. 8 and 9. The maximum efficiency, by the mass mean integration, is shown to have decreased with decreasing diameter ratio, from about 0·90 at a diameter ratio of 0·65 to about 0·87 at a ratio of 0·35. There is still a tendency, especially at the lowest diameter ratio, for the optimum flow to be rather high. The cause of this is unknown, though it may be partly caused by inadequate knowledge of the extra-to-stage losses in the rig. The low-diameter-ratio stage also exhibited a more rapid fall-off in efficiency away from the peak value.

3.4. *Working Range.*—The blade design tested in this family of compressors showed a considerable loss in working range with low diameter ratio. Thus the highest diameter-ratio stage reached a mass-flow coefficient of 0·64 compared with the design value of 0·8 before the flow broke down into a ' warbling surge '. The lowest diameter ratio, however, only reached a flow coefficient of 0·77 before the range of uniform flow was limited by a secondary reverse flow at the outside diameter. This flow regime was replaced at lower flows by a ' warbling ' surge. Traverses after the rotor blade row, plotted in Fig. 10, show the development of the total-head and air-angle distributions during this reverse-flow regime. The high very values of the stator inlet angle, α_3, shown here definitely indicate that low axial velocities exist, confirming the reverse flow referred to above. Further proof of its existence was obtained from visual stroboscopic examination of wool tufts on the blades.

A satisfactory explanation of this phenomenon appears from consideration of the stalling properties of the blades. The stall points of the various blade sections, in terms of V_a/U_m, calculated by the methods of Refs. 4 and 8, are plotted in Fig. 11. Shown also on this Figure are the radial distributions of V_a/U_m assuming the inlet-guide-blade radial-equilibrium velocity distribution (*see* Section 4.4), for the ' stall ' points of the three compressors. It is remarkable that the 0·35-diameter-ratio stage reached the limit of truly stable operation just when the tip section was expected to stall on this simple basis, though the form of the experimental velocity distribution was such that some 10 per cent of the blade must actually have been stalled. As the diameter ratio was increased, the flow did not break down until an increasingly large percentage of the blade was stalled. At the maximum diameter ratio of 0·65, the stage surged when the mid-height of the blade was apparently stalled. This fits in with experience on a high-diameter-ratio compressor[9] and it is to be expected that the lower diameter-ratio stages would be more sensitive to root and tip operating conditions and especially to such instabilities as stalling.

The surge of the low-diameter-ratio stages may be explained as follows :

Stable flow conditions continued until the mass flow was reduced as far as the tip stall in Fig. 11. When this was reached, the pressure rise across the tip dropped off and a secondary reverse flow was set up causing a considerable decrease in axial velocity and increase in stator air-inlet angle near the outer diameter. As the flow was further reduced, this secondary flow spread down the blade until some considerable part (about 60 per cent) was affected, while the inner part of the blade apparently continued to work normally. The flow then broke down into a warbling surge. The nature of this surge was not examined in detail, but the noise was typical of the common rotating surge. With the low-diameter-ratio stage tested, this warbling surge existed only over a very small range of flow. It was very quickly superseded by a further form of secondary flow in which the air was centrifuged outwards in the rotor row with attendant inward radial flow in the stationary rows. When the mass flow and therefore the mean axial velocity was reduced to zero, this latter form of flow was supreme. As the diameter ratio was increased, the flow range of the tip reverse-flow regime was reduced until, at a diameter of 0·65, the tip stall was not sufficiently severe to cause a reverse flow before surge, in spite of the fact already noted that this stage continued to work stably until half of the rotor blade was stalled.

4. *Test Results.—Axial-Velocity Distributions.*—4.1. *General.*—The axial-velocity distributions necessary to satisfy the radial-equilibrium conditions after each blade row have been calculated from first principles by the methods of Appendix II. A large part of the test work has been

directed at an investigation of the degree of agreement with these conditions which was achieved, in order to understand the importance of this criterion for design purposes. These theoretical distributions are plotted in Figs. 12 and 13. It will be seen that equilibrium after the rotor row demands the establishment of distribution having a fairly high negative slope which does not vary greatly with the mass-flow coefficient. After the stator row, however, there is a considerable change of distribution with flow, caused by the increased work done at the tip of the rotor blade when operating in the velocity distribution which gives equilibrium after the inlet guide blades.

4.2. *Before the Inlet Guide Blades.*—The distributions measured at the inlet traversing station 0·4 chords upstream of the inlet-guide-blade leading edges are shown for the three diameter ratios in Fig. 14. Also plotted for comparison are the velocity distributions required for radial equilibrium downstream of the row. It will be seen that the design condition of constant axial velocity was not achieved. Instead, there appears to be a tendency for the flow to adjust itself towards the distribution required for equilibrium downstream of the row. It was also noticed on test that the static pressures measured near the outside diameter were slightly higher than those near the hub.

It is probable that these observations may be explained on purely mechanical grounds. Thus it must be remembered that while the aerodynamic design of the high-diameter-ratio stage is essentially a ' slice ' symmetrical about the mean diameter of the low-diameter-ratio stage, mechanically the flow annulus is a ' slice ' at the outer diameter, since in all cases the outer casing is the same. Apart from the effects of the different degrees of acceleration from the compressor entry to the working-section, the boundary layer on this casing may be expected to be substantially similar for all three compressors. If the inlet velocity profiles are compared on this basis, the differences between them are considerably reduced. It is possible also that the lower static pressures near the hub are caused by the rapid acceleration on the hub near to the working-section.

It is possible, however, that some of this effect may be caused by a tendency for the flow upstream of a blade row to begin to adjust itself towards the distribution required for equilibrium downstream of the row, but there is no strong evidence supporting this suggestion.

4.3. *After the Inlet Guide Blades.*—Fig. 15 shows the distributions measured after the inlet guide blades at three positions on the compressor characteristic, *viz.*, near maximum flow at flow coefficient of approximately 1·0, near the design value of 0·8 and (except for the compressor of diameter ratio 0·35) at a value about 0·7, near the surge point.

These distributions show that there was a slight shift of the axial-velocity distribution through the blade row towards that required for radial equilibrium at all diameter ratios, although the actual magnitude of the change was small. There is evidence that a closer approximation to equilibrium is achieved at high diameter ratios than at low and a slight tendency to better agreement near the surge point especially at high diameter ratios.

These results agree with earlier work by Carter[10] in which he found that, with accelerating blades in an annulus of diameter ratio approximately 0·6, equilibrium was set up very quickly.

4.4. *After the Rotor Blades.*—At all diameter ratios, Fig. 16 shows that the axial-velocity distributions again changed through the blade row towards that required for equilibrium downstream of the row, though this theoretical condition is not achieved. The theoretical curve for design flow is plotted on Fig. 16 as typical of the distribution required. The change of profile through the row was only some 30 per cent of that required, and left the outlet distribution still very similar to that required for equilibrium after the inlet guide blades.

It is interesting to note that these distributions are very much alike at all diameter ratios : especially noticeable is the similarity between the distributions for the diameter ratios of 0·5 and 0·65, when compared with the difference between the corresponding distributions after the stator blades (*see* Fig. 17). These traverses after the rotor row are the only ones of this series

which do not show a closer approximation to equilibrium conditions at high diameter ratios than at low. It is suggested that this is caused by the partial satisfaction upstream of a blade row of the conditions required for equilibrium downstream of the row. The slight tendency towards a higher negative slope of the velocity distribution near to surge than near to maximum flow may be further evidence in favour of this suggestion. This effect appears to be somewhat stronger upstream of a stator row than a rotor row, from examination of the distribution after the inlet guide blades.

It may be that part of this similarity of profiles may be attributed to the extra centrifugal effects which are present in a rotor row. It is possible that these may in some way resist any great increase in flow near the inside diameter especially at high diameter ratios, but this phenomenon is not well understood.

4.5. *After the Stator Blades.*—Two sets of measured distributions after the stator row are available : those computed from traverses 0·4 chords downstream of the blade trailing edges and those obtained from the total-head distributions measured at the pitot combs 2·5 chords downstream. The latter calculations assumed design air-outlet angles and a linear variation of static pressure between inner and outer wall tappings. These two sets are plotted in Figs. 17 and 18. Also plotted for comparison are the theoretical radial-equilibrium distributions for design mass flow and near maximum flow.

It will be seen that in each case there was a change of velocity distribution from that measured after the rotor row towards that required for equilibrium down stream of the stator row. In more detail, the results show the following :

At the low diameter ratio, there was a slight change through the blade row, with very little further change downstream within the distance to the pitot combs.

At the medium diameter ratio, there was a slightly greater change through the blade row, followed by a considerable change towards equilibrium before the pitot combs, especially at the low-mass-flow end of the characteristic, where equilibrium demands the maximum change of distribution.

At the high diameter ratio, a very marked shift takes place within the blade row, with only a small change downstream of the row. Even at the maximum diameter ratio of these tests, 0·65, radial equilibrium was not fully established, according to these curves, but it is not known to what extent this is due to conditions upstream of the stator not being as fully developed as was assumed in the theoretical calculations.

These results indicate that the establishment of radial equilibrium after a blade row requires an axial distance which increases with decreasing diameter ratio. It seems probable that with the axial spacing between blade rows typical of full scale compressors, equilibrium may be assumed to be set up with diameter ratios higher than 0·65, but with low diameter ratios of about 0·35, this will only be true if the change of velocity distribution required is small.

5. *Prediction of Performance.*—The comparison of Section 3 between the experimental characteristics and those obtained by the standard methods of performance estimation showed that these methods were inadequate for the estimation of the performance of a low-diameter-ratio stage, although agreement was reasonable at high diameter ratios. The detailed results of the previous Section, however, suggested that a good approximation to the conditions through the rotor row would be to assume radial equilibrium to be satisfied after the inlet guide blades with no change of velocity distribution through the rotor row. Characteristics have accordingly been calculated on this assumption, by the integration of the performances of the various sections of the blade. As before, this integration has been carried out in two ways, by ' radial mean ' and ' mass mean ' methods, and the results are plotted in Figs. 19, 20 and 21.

The two methods of computation show very little difference in the design-point performance, or in the efficiency characteristics of the stages, but an appreciable difference appears in the slopes of the temperature rise characteristics. The methods are compared with the standard calculation and the experimental results in the following Table :

		Diameter ratio		
		0·65	0·5	0·35
Test results	Design flow $\frac{K_p \Delta T}{\frac{1}{2}U_m^2}$	+1·056	+1·088	+1·093
	Slope	−0·99	−1·11	−1·22
Standard calculation	Design flow $\frac{K_p \Delta T}{\frac{1}{2}U_m^2}$	+1·06	+1·06	+1·06
	Slope	−1·39	−1·39	−1·39
Mass mean integration	Design flow $\frac{K_p \Delta T}{\frac{1}{2}U_m^2}$	+1·072	+1·089	+1·114
	Slope	−1·45	−1·56	−1·77
Radial mean integration ..	Design flow $\frac{K_p \Delta T}{\frac{1}{2}U_m^2}$	+1·070	+1·082	+1·095
	Slope	−1·40	−1·42	−1·47
$\Omega_0 = 0{\cdot}925$ (corrected)	Slope	−1·11	−1·19	−1·36

For the work done at design flow, while there is relatively little to choose between the radial and mass-mean integrations, the best method of predicting the performance appears to be the use of the mass-mean values in conjunction with the normal work-done factor of 0·98.

The change of slope of the experimental temperature rise characteristic with diameter ratio is best predicted by the mass-mean integration, which should give the best result. However, the experimental slope is much less arithmetically than that predicted by any of the theoretical methods. This has been observed on many full-scale compressors by Carter in Ref. 7.

Carter shows that for many full-scale compressors the work-done characteristic may be approximated to by a straight line drawn through intercepts of $2\Omega_0$ 1/(tan α_0 + tan α_2) on the temperature-rise-coefficient and mass-flow-coefficient scales respectively. The analysis in Ref. 7 of results of tests on two sets of blading in a low-speed compressor of diameter ratio 0·75 suggests that for a first stage, Ω_0 should be taken as 0·925 and the design outlet angles used. For the present blading design, this method suggests a slope of — 1·09, but the very low work-done factor at design flow of 0·925. However, using this value for the slope of the curve at a diameter ratio of 0·75 and correcting it for lower diameter ratios by the percentage change predicted by the mass-mean integration, gives the values of slope shown in the last line of the above Table. This semi-empirical method gives the nearest approach to the experimental results, but the differences indicate that while it may be of use at present for estimating the slope of the curve, the method is not fully adequate, and considerable further information is necessary before the characteristic can be fully predicted with confidence.

Since the efficiencies calculated by the two integration methods differ only very slightly, it may be said that the most satisfactory method available at present for estimating the overall characteristics of a low-diameter-ratio stage is by mass-mean integration of the blade-section performance provided that the temperature and pressure-rise characteristics are decreased in slope according to the empirical correction referred to.

As remarked in Section 2.4, it is probable that correction of the experimental results to higher Reynolds numbers would increase the efficiency slightly. Corresponding increases in the estimated efficiencies could result from some reduced allowance for secondary losses, etc., at reduced diameter ratios.

6. *Design Recommendations and Discussion.*—It has been shown that the simple blade design tested suffered considerable variation of performance with diameter ratio. Indications have also been found, however, whereby it is to be expected that much of this variation can be avoided by appropriate design methods. Thus it has been shown that a good velocity distribution to assume for design purposes is that which satisfies radial equilibrium after the inlet guide blades, provided that these are designed to give the same air outlet angles as the stator blades. If then the rotor row is designed to give the same work done at all blade heights, Appendix II shows that the changes in velocity distribution through the blade rows necessary to satisfy radial equilibrium are reduced to a minimum and an adequate approximation to the flow is to assume no change in distribution through the stage.

The working range of such a stage can then be estimated from consideration of the stalling properties of the blade sections. Section 3.4 suggested that the stall or surge of the stage could be delayed if at least the upper part of the stalling characteristic of Fig. 11 could be moved towards lower values of V_a/U_m. An approximate design of a rotor blade has been evolved, based on the method of the previous paragraph, and the stalling characteristic of this blade is shown in Fig. 11. A considerable shift in the required direction has been achieved. A further improvement can be obtained with this form of design by an alteration in the method of blade design from the air angles. So far in these designs, the various blade sections have been designed as far as possible to operate at nominal conditions. At the high staggers and low cambers near the outer diameter this has resulted in rather high design incidences. It is probable[11] that a high-speed design would use incidences nearer to zero in the interests of efficient high-Mach-number operation, and the corresponding higher cambers would have a somewhat later two-dimensional stall. This modification has been carried out on the improved design referred to above and the resulting stalling characteristic is also shown in Fig. 11. If this simple tip-stalling hypothesis is sufficient to explain and predict the working range, this modified design method should enable a stage of diameter ratio 0·35 to have the same stall or surge point as that shown by the present design at a diameter ratio of about 0·5. One factor which will tend to reduce the working range of a practical high-speed design is the taper in chord which is likely for stress reasons, with the attendant higher pitch/chord ratios near the tip and earlier stall.

Since it is important that the early stages of a compressor, where the diameter ratio tends to be low, should have a good working range at flow coefficients below design rather than above, it may well be advisable to extend this practice of designing the blade sections below nominal conditions to include the mean-diameter cascades, subject always to efficient operation at high Mach numbers. There are two points, however, relative to the stalling properties of this type of design. Firstly, the long blades associated with low diameter ratios are rather susceptible to flutter and this problem may be aggravated by designing in such a manner that a large part of the outer half of the rotor blade may be expected to stall at the same flow. Secondly, there is a possibility that this same characteristic may cause a tendency to an early surge of the compressor. Thus a row designed so that a definite part of the blade, say the tip, stalls first, may enable a partial reverse flow to be set up in the neighbourhood of the stalled portion, possibly delaying the main compressor surge.

If all blade sections were designed at nominal conditions with the velocity distribution which would be obtained on test, then the various sections may be expected to reach their peak efficiency at the same flow. The static-pressure-rise characteristics, which appear to be influenced by the tip-section preformance, should therefore show very little change in optimum flow with diameter ratio. The variation of flow for peak total-pressure efficiency is a little uncertain, but it is considered probable that this also would show little change. With the blade design tested, there was some fall-off in maximum total-pressure efficiency with decreasing diameter ratio due largely

to mis-matching of the various blade sections with the velocity distribution obtained on test. With this ' nominal ' design, this should not occur, and the peak efficiency may be expected to be both slightly higher and also less dependent on diameter ratio, though this would only be achieved at the expense of a more rapid fall-off in efficiency away from the peak.

Designing for conditions below nominal on the outer part of the blade will tend to move the peak efficiency towards lower flows at low diameter ratios and also to flatten out the characteristics slightly.

With this method of design, the work done at design flow will be almost independent of diameter ratio, but off design, the slope of the characteristic will still change. This will probably be best forecast by the method of Section 5, *i.e.*, using mass mean integration of the blade-section performance for design-point temperature rise and the change in slope with diameter ratio, coupled with the empirical correction for slope derived from Ref. 7. This mass-mean-integration technique probably gives the best method for the evaluation of efficiency and pressure rise, but the difference between the various methods of integration is likely to be small. This difference depends on the variation in the blade-section characteristics and hence the diameter ratio, and also very largely on the form of the axial velocity distribution. Thus if rV_a is independent of r, then the mass and radial mean calculations give the same result.

It is obvious, however, that these methods of predicting the stage performance are not complete, and further information is needed, especially as to the factors controlling the slope of the work-done characteristic, and such other matters as the variation of secondary loss with diameter ratio.

7. *Conclusions.*—(1) These tests on a simple low-stagger blade design based on constant axial velocity and constant α_3 have shown considerable variation of stage performance with change of diameter ratio over the range from 0·65 to 0·35.

(2) These variations were :

(*a*) A slight increase in work done at design flow and considerable increase in slope of the work-done characteristic as the diameter ratio was reduced.

(*b*) A decrease of peak total-pressure efficiency of about 3 per cent, together with more rapid fall-off of efficiency away from the peak, as the diameter ratio was reduced from 0·65 to 0·35.

(*c*) A considerable reduction of stable working range with decrease of diameter ratio.

(3) The satisfaction of radial equilibrium conditions requires an axial distance which increases considerably with decrease in diameter ratio such that, while at high diameter ratios equilibrium can be assumed to be set up within the axial spacing between blade rows of a typical compressor, this is only true at low diameter ratios if the changes in velocity distribution required are small.

(4) There is evidence that the pressure rise measured by static tappings on the outside diameter of the flow annulus is appreciably influenced by the characteristic of the tip section of the blades.

(5) It is suggested that conditions upstream of a stator blade row are noticeably influenced by the conditions required for radial equilibrium downstream of that row.

(6) It is recommended that, at least for low stagger constant α_3 stages and probably other forms of design as well, a low-diameter-ratio stage should be designed on the basis of a radial distribution of axial velocity which will satisfy radial equilibrium after the inlet guide blades, and with constant work done at all sections of the rotor blade.

(7) The loss of working range of a low-diameter-ratio stage may be minimized by designing at least the outer half of the blades as far below nominal conditions as such considerations as blade taper and high-Mach-number operation will allow. The surge point of the stage can then be estimated from consideration of the stalling properties of the blade sections.

(8) The performance of such a stage is best predicted by integrating the strip performances of the various sections of the blade. Integration by the ' mass mean ' method gives the best result, but further information is needed, particularly regarding the slope of the work-done characteristic, before the performance can be accurately calculated.

NOTATION

a	Blade speed/axial velocity, U/V_a, at mean radius
A	Design value of a
c	Blade chord
r	Radius ratio, radius/mean radius
r_1	Value of r at outside radius of annulus
r_2	Value of r at inside radius of annulus
s	Blade pitch
ΔT	Total temperature rise
Δp	Static-pressure rise
ΔP	Total-pressure rise
V	Air velocity
U	Blade speed
α	Air angle measured from axial direction
θ	Blade camber
ζ	Blade stagger
ρ	Air density
η_{is}	Isentropic efficiency
Ω	Work-done factor as defined in Ref. 2
Ω_0	Work-done factor as defined in Ref. 7
Tan α	Design value of tan α
$\bar{V}_a$	Mass mean axial velocity

Subscripts

$_0$ (except on Ω)	At exit from inlet guide blades
$_1$ (except on r)	At entry to rotor blades
$_2$ (except on r)	At exit from rotor blades
$_3$	At entry to stator blades
$_4$	At exit from stator blades
$_a$	Axial
$_w$	Whirl
$_r$	At radius r
$_m$	At mean radius

REFERENCES

No.	Author	Title, etc.
1	G. L. Shires..	On a type of air-lubricated journal bearing. C.P. 318. November, 1949.
2	A. R. Howell	Fluid dynamics of axial comp ressors. *Proc. Inst. Mech. Eng.* Vol. 153. p. 447. 1945.
3	A. D. S. Carter	The low-speed performance of related aerofoils in cascade. C.P. 29. September, 1949.
4	A. D. S. Carter and A. F. Hounsell	General performance data for aerofoils having C.1, C.2 or C.4 base profiles on circular arc camber lines. A.R.C. 12,889. August, 1949.
5	R. A. Jeffs	Preliminary note on the performance of axial compressor blading designed to operate in a radially varying axial velocity distribution. R. & M. 2929. July, 1949.
6	A. R. Howell and R. P. Bonham	Overall and stage characteristics of axial flow compressors. *Proc. Inst. Mech. Eng.* Vol. 163. pp. 235 to 248. 1950.
7	A. D. S. Carter	A note on the ' Work Done Factor '. A.R.C. 14,635. August, 1951.
8	R. A. Jeffs, A. F. Hounsell and R. G. Adams	Further performance data for aerofoils having C.1, C.2 or C.4 base profiles on circular arc camber lines. A.R.C. 14,755. December, 1951.
9	R. A. Jeffs, E. L. Hartley and P. Rooker	Tests on a medium stagger free vortex blading with various stator blade staggers. C.P. 132. September, 1950.
10	A. D. S. Carter	Vortex wind tunnel.—Tests on various vortex flows. Power Jets Report R.1063. January, 1945.
11	A. D. S. Carter and Hazel P. Hughes	Note on the high-speed performance of compressor cascades. A.R.C. 12,197. December, 1948.
12	H. Cohen and Elizabeth M. White	The theoretical determination of the three-dimensional flow in an axial compressor with special reference to constant reaction blading. A.R.C. 6842. April, 1943.

APPENDIX I

Blade Design

The major design criteria were as follows :

(*a*) Work done, ΔT, constant at all radii

(*b*) Axial velocity, V_a, constant at all radii

(*c*) Stator air inlet angle, α_3, constant at all radii

(*d*) Blade chord, c, constant at all radii

(*e*) 50 per cent reaction at mean radius

(*f*) Pitch/chord ratio, s/c, equal to 0·9 at mean radius

(*g*) Blade-speed axial velocity, U/V_a, at mean radius = 1·25

(*h*) Deflection at mean radius given by

$$\tan \alpha_1 - \tan \alpha_2 = \frac{1 \cdot 55}{1 + 1 \cdot 5 s/c} \qquad \text{(Ref. 3)}$$

(*i*) Outlet air angles from stator and inlet guide blade are identical.

Item (*e*) was decided upon as the result of a theoretical investigation into the effect of varying the radius of 50 per cent reaction from the inside radius to the mean radius. It was found that having this criterion at mean radius gave the least arduous tip conditions for high-speed operation, with the design condition of constant axial velocity.

These conditions are sufficient to define the air angles. As far as was possible, the blade angles were then determined by the methods of Refs. 4 and 5, so that all blade sections should operate at nominal conditions. Actually, the very highly cambered sections near the inside diameter of the low-diameter-ratio stage were designed somewhat above nominal conditions. Throughout, the C.5 base profile has been used on circular-arc camber lines.

The resulting cambers and staggers of the blade sections for the stage of diameter ratio 0·35 are given in the following Table. The blades for the higher diameter ratios are obtained essentially by a ' slice ' out of the centre of these blades, though very slight differences occur due to the number of blades, etc., these blades having been designed for constant chord for all blades in each compressor.

Diameter ratio 0·35 — Blade chord 2·01 in.

Blade detail	Number of blades	Radius ratio r						
		0·55	0·65	0·8	1·0	1·2	1·35	1·45
Rotor	23							
Camber θ		+75·3	+68·5	+58·2	+44·5	+28·8	+14·4	+ 3·5
Stagger ζ		−10·0	−13·6	−19·7	−27·6	−34·5	−38·8	−41·3
Pitch/chord ratio s/c		+ 0·506	+ 0·598	+ 0·736	+ 0·92	+ 1·104	+ 1·242	+ 1·335
Stator	24							
Camber θ		+76·2	+67·3	+56·0	+43·5	+36·7	+29·8	+24·7
Stagger ζ		−11·8	−17·4	−22·5	−27·6	−30·4	−31·3	−31·5
Pitch/chord ratio s/c		+ 0·485	+ 0·572	+ 0·705	+ 0·88	1·057	+ 1·19	+ 1·277
Inlet Guide	24							
Camber θ		+11·5	+ 2·8	+ 6·0	+14·8	+22·0	+26·9	+29·7
Stagger ζ		+ 9·5	+ 3·4	+ 3·8	+10·7	+14·8	+17·2	+18·2
Pitch/chord ratio s/c		+ 0·485	+ 0·572	+ 0·705	+ 0·88	+ 1·057	+ 1·19	+ 1·277

APPENDIX II

Radial Equilibrium Calculations

1. *Basic Assumptions.*—The analysis is based on the following assumptions :

(i) The air outlet angles relative to the blade rows are assumed independent of the incidence onto the blades.

(ii) The total head and axial velocity are assumed constant across the annulus at entry to the inlet guide blades.

(iii) The losses through each blade row are zero.

(iv) At any radius, there is no change of total head relative to a blade row, through that row. This is only true, subject to (iii), along a streamline, and an unknown but probably small error is introduced by the radial flows which take place through each row.

(v) Only asymptotic radial equilibrium is considered, *i.e.*, where the radial velocities are zero.

2. *Blade-Design Equations.*—Using the Notation and the criteria set out in Appendix I, these equations become :

At mean radius, *i.e.*, where $r = 1$

$$\tan \alpha_0 = \tan \alpha_2 = \tan \alpha^4$$

$$\tan \alpha_1 = \tan \alpha_3$$

$$(\tan \alpha_0 + \tan \alpha_1)_m = (\tan \alpha_2 + \tan \alpha_3)_m = \frac{U_m}{V_a} = a \, .$$

At other radii

$$(\tan \alpha_1 - \tan \alpha_2)_r \, xr = (\tan \alpha_1 - \tan \alpha_2)_m$$

and hence

$$\tan \alpha_2 = ar - \tan \alpha_3$$

$$\tan \alpha_0 = \tan \alpha_4 = \frac{a}{r} - \left(\frac{2}{r} - 1\right) \tan \alpha_3 \, .$$

Since these air angles will be assumed independent of a in the following analysis,

$$\tan \alpha_2 = Ar - \mathrm{Tan} \, \alpha_3$$

$$\tan \alpha_0 = \tan \alpha_4 = \frac{A}{r} - \left(\frac{2}{r} - 1\right) \mathrm{Tan} \, \alpha_3 \, ,$$

where capitals denote the design values of a and $\tan \alpha_3$,

then

$$\frac{d}{dr} \tan \alpha_2 = A \, ,$$

$$\frac{d}{dr} \tan \alpha_0 = \frac{(2 \, \mathrm{Tan} \, \alpha_3 - A)}{r^2} \, .$$

3. *Basic Radial Equilibrium Equations.*—The equation for the asymptotic radial equilibrium condition is

$$\frac{1}{\rho} \frac{dp}{dr} = \frac{V_w^2}{r} \, .$$

The distribution of energy is

$$\frac{dH}{dr} = V_w \frac{d\,.\,V_w}{dr} + V_a \frac{d\,.\,V_a}{dr} + \frac{1}{\rho}\frac{dp}{dr}\,.$$

Eliminating the static-pressure term, the basic equation appears

$$\frac{dH}{dr} = \frac{V_w^2}{r} + V_w \frac{d\,.\,V_w}{dr} + V_a \frac{d\,.\,V_a}{dr}. \quad .. \quad .. \quad .. \quad .. \quad (1)$$

This equation is now applied in a manner similar to that in Ref. 12.

4. *Flow after the Inlet Guide Blades.*—From the velocity triangle,

$$V_{w0} = V_{a0} \tan \alpha_0\,.$$

Substituting this in equation (1) and putting $dH_0/dr = 0$,

$$\frac{V_{a0}^2 \tan^2 \alpha_0}{r} + V_{a0} \tan \alpha_0 \left[V_{a0} \frac{d\,.\,\tan \alpha_0}{dr} + \tan \alpha_0 \frac{d\,.\,V_{a0}}{dr}\right] + V_{a0} \frac{d\,.\,V_{a0}}{dr} = 0\,.$$

This simplifies to

$$\frac{d\,.\,V_{a0}}{dr} = -\frac{V_{a0} \operatorname{Tan} \alpha_3 \quad \sin 2\alpha_0}{2r}$$

and

$$\log_e \frac{V_{a0}}{V_{a0m}} = \frac{\operatorname{Tan} \alpha_3}{2} \int_r^1 \frac{\sin 2\alpha_0}{r}\, dr\,. \quad .. \quad .. \quad .. \quad .. \quad .. \quad (2)$$

The integration was performed graphically and the resulting distribution is shown plotted in Fig. 11.

5. *Flow after the Rotor Blades.*—In this case, the velocity triangle gives

$$V_{w3} = U - V_{a2} \tan \alpha_2$$

and the basic equilibrium equation becomes, after a little simplification,

$$\frac{dH_2}{dr} = \frac{2U^2}{r} + \frac{d\,.\,V_{a2}}{dr}\left[V_{a2} \sec^2 \alpha_2 - U \tan \alpha_2\right] - UV_{a2}\left[\frac{3 \tan \alpha_2}{r} + \frac{d\,.\,\tan \alpha_2}{dr}\right] +$$
$$+ V_{a2}^2 \tan \alpha_2 \left[\frac{d\,.\,\tan \alpha_2}{dr} + \frac{\tan \alpha_2}{r}\right]. \quad .. \quad .. \quad .. \quad .. \quad .. \quad .. \quad (3)$$

Also the work done through the rotor is

$$\Delta H = H_2 - H_0 = U(V_{w3} - V_{w0})$$
$$= U(U - V_{a2} \tan \alpha_2 - V_{a0} \tan \alpha_0)\,.$$

Differentiating this and putting $dH_0/dr = 0$, we have a second equation for dH_2/dr. This becomes

$$\frac{dH_2}{dr} = \frac{2U^2}{r} - U \tan \alpha_2 \frac{d\,.\,V_{a2}}{dr} - UV_{a2}\left[\frac{\tan \alpha_2}{r} + \frac{d\,.\,\tan \alpha_2}{dr}\right] - U \tan \alpha_0 \frac{d\,.\,V_{a0}}{dr} -$$
$$- UV_{a0}\left[\frac{\tan \alpha_0}{r} + \frac{d\,.\,\tan \alpha_0}{dr}\right]. \quad .. \quad .. \quad .. \quad .. \quad .. \quad .. \quad .. \quad (4)$$

Equating these two values of dH_2/dr, we have after some simplification

$$\frac{d\,.\,V_{a2}}{dr} = \cos^2\alpha_2\left[\frac{2U\tan\alpha_2}{r} - V_{a2}\tan\alpha_2\left(2A - \frac{\mathrm{Tan}\,\alpha_3}{r}\right) - \frac{UV_{a0}\,\mathrm{Tan}\,\alpha_3\quad\cos^2\alpha_0}{V_{a2}r}\right].$$

Dividing by $\bar{V}_a$ and putting

$$\frac{U}{\bar{V}_a} = \frac{U_m}{\bar{V}_a}r = ar\,,$$

$$\frac{d\,.\,V_{a2}}{dr} = \cos^2\alpha_2\left[2a\tan\alpha_2 - \frac{V_{a2}}{\bar{V}_a}\tan a_2\left(2A - \frac{\mathrm{Tan}\,\alpha_3}{r}\right) - \frac{aV_{a0}\,\mathrm{Tan}\,\alpha_3\quad\cos^2\alpha_0}{V_{a2}}\right] \quad . . \qquad (5)$$

and

$$\frac{V_{a2}}{\bar{V}_a} - \frac{V_{a2m}}{\bar{V}_a} = \int_1^r \cos^2\alpha_2\left[2a\tan\alpha_2 - \frac{V_{a2}}{\bar{V}_a}\tan\alpha_2\left(2A - \frac{\mathrm{Tan}\,\alpha_3}{r}\right) - \frac{aV_{a0}\,\mathrm{Tan}\,\alpha_3\quad\cos^2\alpha_0}{V_{a2}}\right]dr\,. \quad . . \quad . . \quad . . \quad . . \quad . . \qquad (6)$$

The integration was solved by successive approximation and the resulting distributions for various values of a are plotted in Fig. 11.

6. *Flow after the Stator Blades.*—Here the whirl velocity is

$$V_{w4} = V_{a4}\tan\alpha_4 = V_{a4}\tan\alpha_0 \text{ (by design)}$$

and

$$\frac{dH_4}{dr} = \frac{dH_2}{dr} \text{ (by assumptions (iii) and (iv) above).}$$

Then the basic equation (1) becomes

$$\frac{dH_2}{dr} = V_{a4}\frac{d\,.\,V_{a4}}{dr}\sec^2\alpha_0 + \frac{V_{a4}^2\tan\alpha_0\quad\mathrm{Tan}\,\alpha_3}{r}$$

or

$$\frac{2\cos^2\alpha_0}{\bar{V}_a^2}\frac{dH_2}{dr} = \frac{d}{dr}\left(\frac{V_{a4}}{\bar{V}_a}\right)^2 + \frac{V_{a4}^2\,\mathrm{Tan}\,\alpha_3\quad\sin 2\alpha_0}{\bar{V}_a^2 r}\,. \quad . . \quad . . \quad . . \quad . . \qquad (7)$$

Integration of this equation gives

$$\left(\frac{V_{a4}}{\bar{V}_a}\right)^2 - \left(\frac{V_{am}}{\bar{V}_a}\right)^2 = \frac{2}{J}\int_1^r \frac{J\cos^2\alpha_0}{\bar{V}_a^2}\frac{dH_2}{dr}\,dr\,, \quad . . \quad . . \quad . . \quad . . \quad . . \quad . . \qquad (8)$$

where the integrating factor J is given by

$$J = e^{\mathrm{Tan}\,\alpha_3\int_1^r \frac{\sin 2\alpha_0}{r}\,dr}$$

and dH_2/dr is found as in Section 6, equation (4).

Thus, substituting for $d\,.\,V_{a2}/dr$ from equation (5) this reduces to

$$\frac{dH_2}{dr} = \frac{2U^2\cos^2\alpha_2}{r} - UV_{a2}\cos^2\alpha_2\left[2A - \frac{\mathrm{Tan}\,\alpha_3}{r}\right] - \frac{UV_{a0}\,\mathrm{Tan}\,\alpha_3\quad\cos^2\alpha_0}{r}\left[1 - \frac{u\tan\alpha_2\quad\cos^2\alpha_2}{V_{a2}}\right].$$

Dividing by $\bar{V}_a^2$ and putting $U/\bar{V}_a = ar$,

$$\frac{1}{\bar{V}_a^2}\frac{dH_2}{dr} = a\left[2ar\cos^2\alpha_2 - \frac{V_{a2}}{\bar{V}_a}r\cos^2\alpha_2\left(2A - \frac{\mathrm{Tan}\,\alpha_3}{r}\right)\right] -$$

$$- \frac{V_{a0}}{\bar{V}_a}\mathrm{Tan}\,\alpha_3 \quad \cos^2\alpha_0\left[1 - \frac{ar\tan\alpha_2 \quad \cos^2\alpha_2}{V_{a2}/\bar{V}_a}\right]. \qquad .. \qquad .. \qquad (9)$$

Since for a given value of a the distributions of V_{a0} and V_{a2} are already known, the calculation of V_{a4} is by simple graphical integration. The distributions for various values of a are plotted in Fig. 12.

Note.—If dH_2/dr is put equal to zero, the distribution after the stator blades reduces to that after the inlet guide blades, since equation (7) becomes

$$\frac{d}{dr}\left(\frac{V_{a4}^2}{\bar{V}_a^2}\right) + \frac{V_{a4}^2}{\bar{V}_a^2}\frac{\mathrm{Tan}\,\alpha_3 \quad \sin 2\alpha_0}{r} = 0\,,$$

$$\log_e\frac{V_{a4}}{V_{am}} = \frac{\mathrm{Tan}\,\alpha_3}{2}\int_r^1\frac{\sin 2\alpha_0}{r}\,dr\,, \qquad .. \qquad .. \qquad .. \qquad .. \qquad .. \qquad .. \qquad (10)$$

which is identical to equation (2).

The equation for the distribution after the stator can therefore be written in the general form

$$\frac{d\,.\,V_{a4}}{dr} = \frac{d\,.\,V_{a0}}{dr} + f\left(\frac{dH_2}{dr}\right)$$

and it appears that a rotor blade designed for the same work done at all radii with radial equilibrium after the inlet guides would cause the minimum change of velocity distribution through the following stator row.

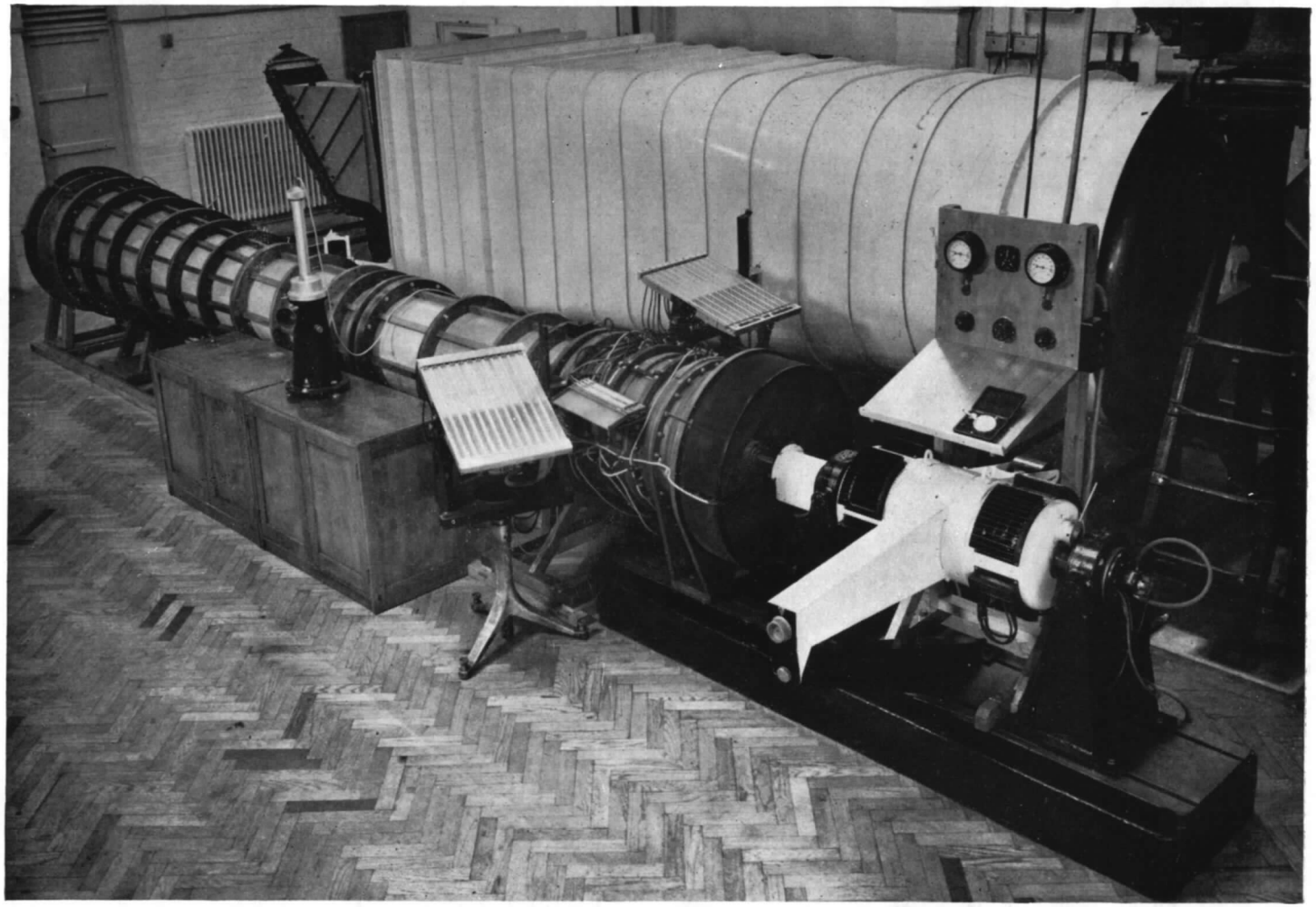

FIG. 1. General view of test rig.—C.123.

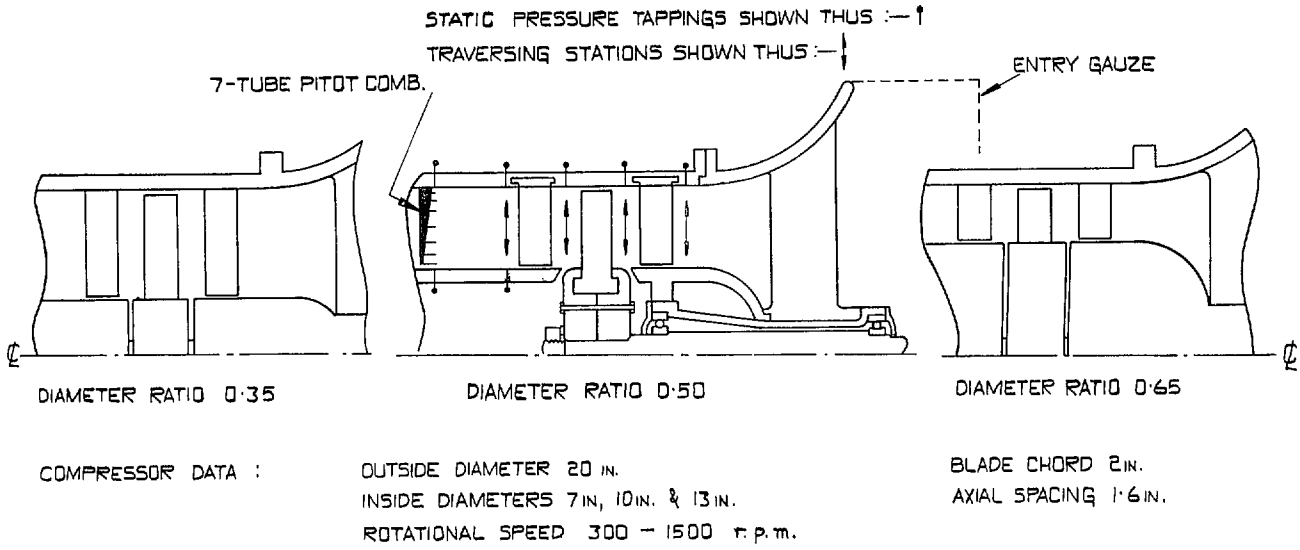

FIG. 2. Diameter-ratio compressor test rig.—C.123.

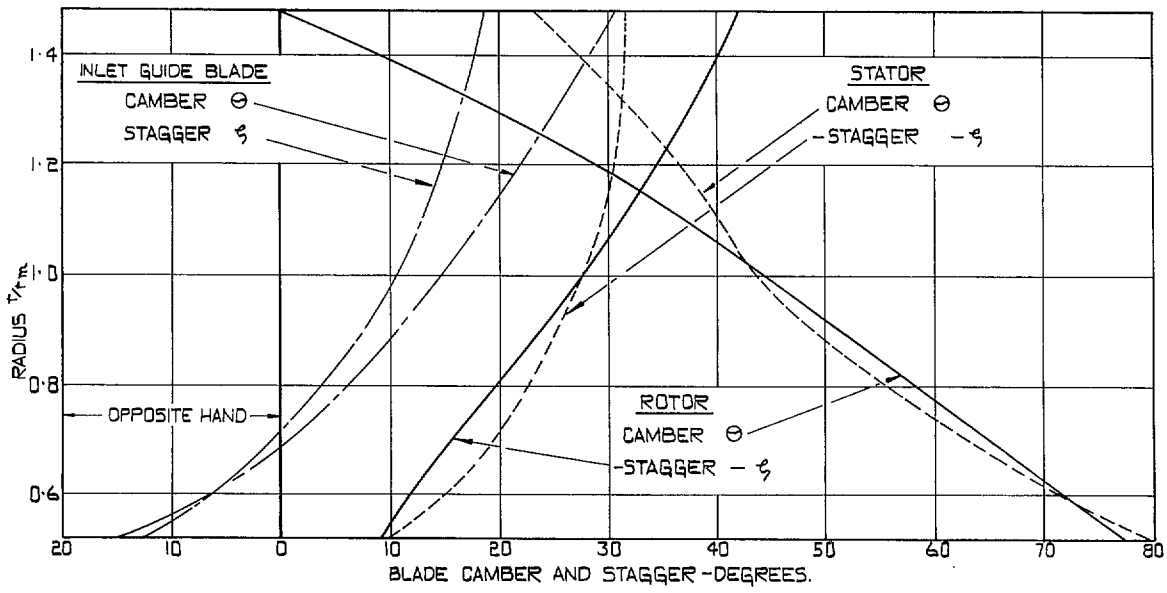

FIG. 3. Blade details.

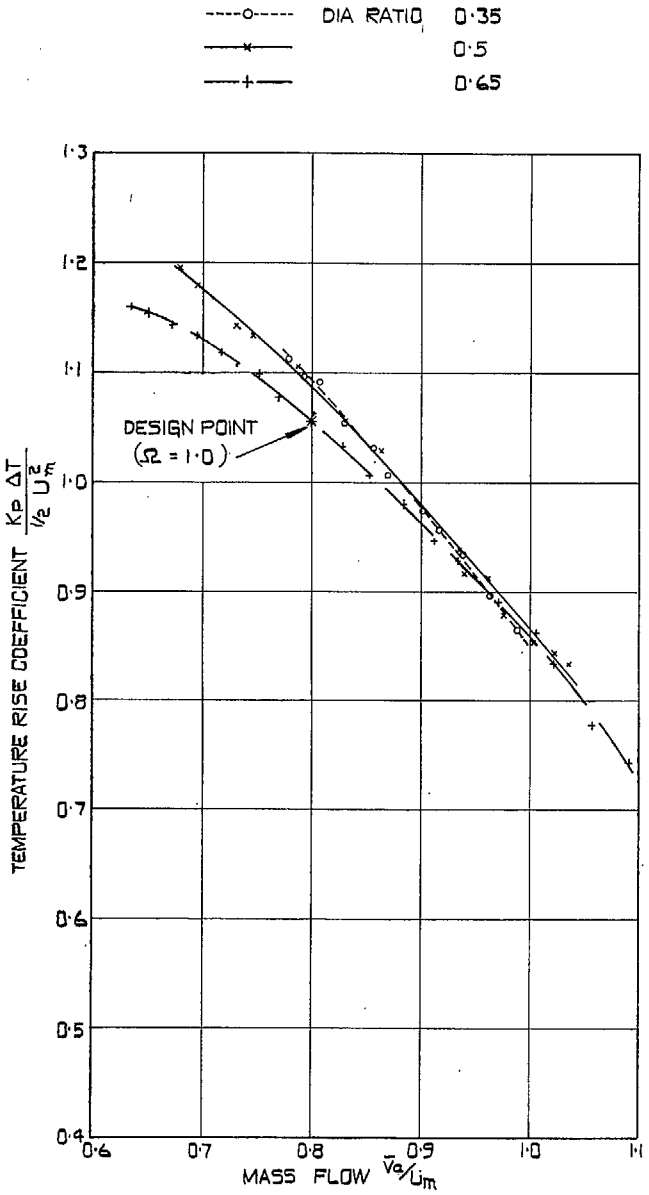

FIG. 4. Experimental temperature-rise characteristics.

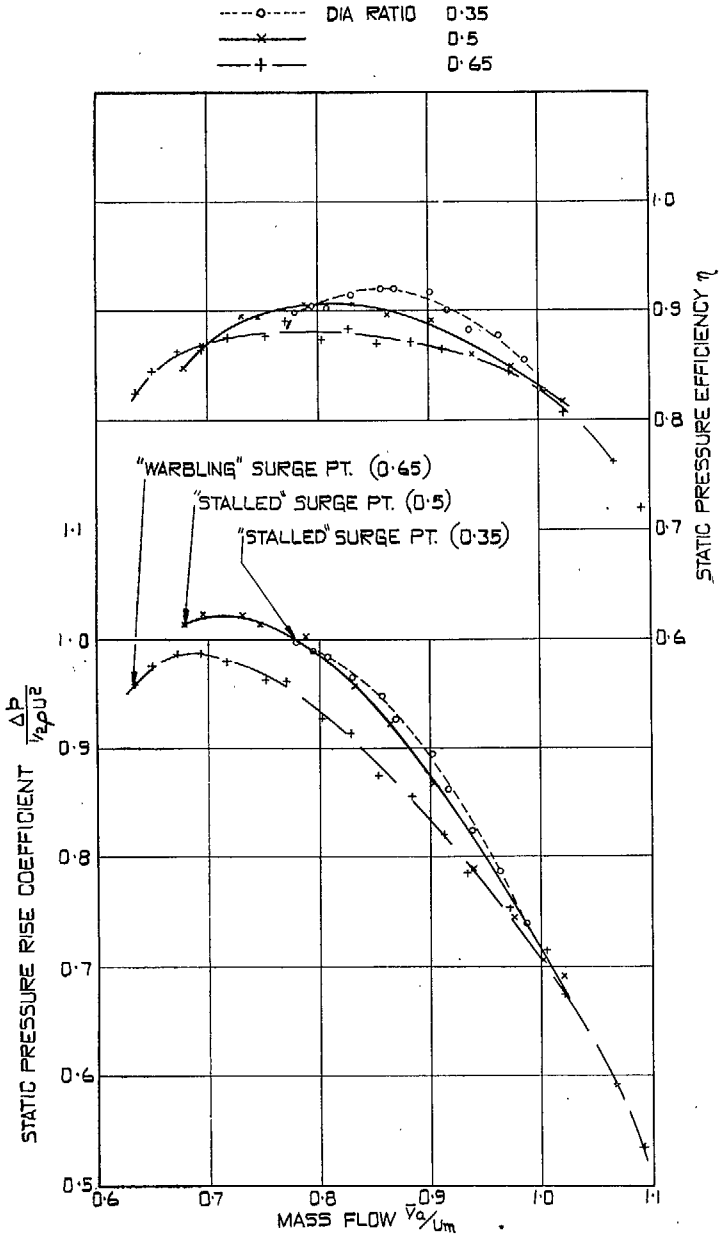

FIG. 5. Experimental characteristics based on static-pressure rise.

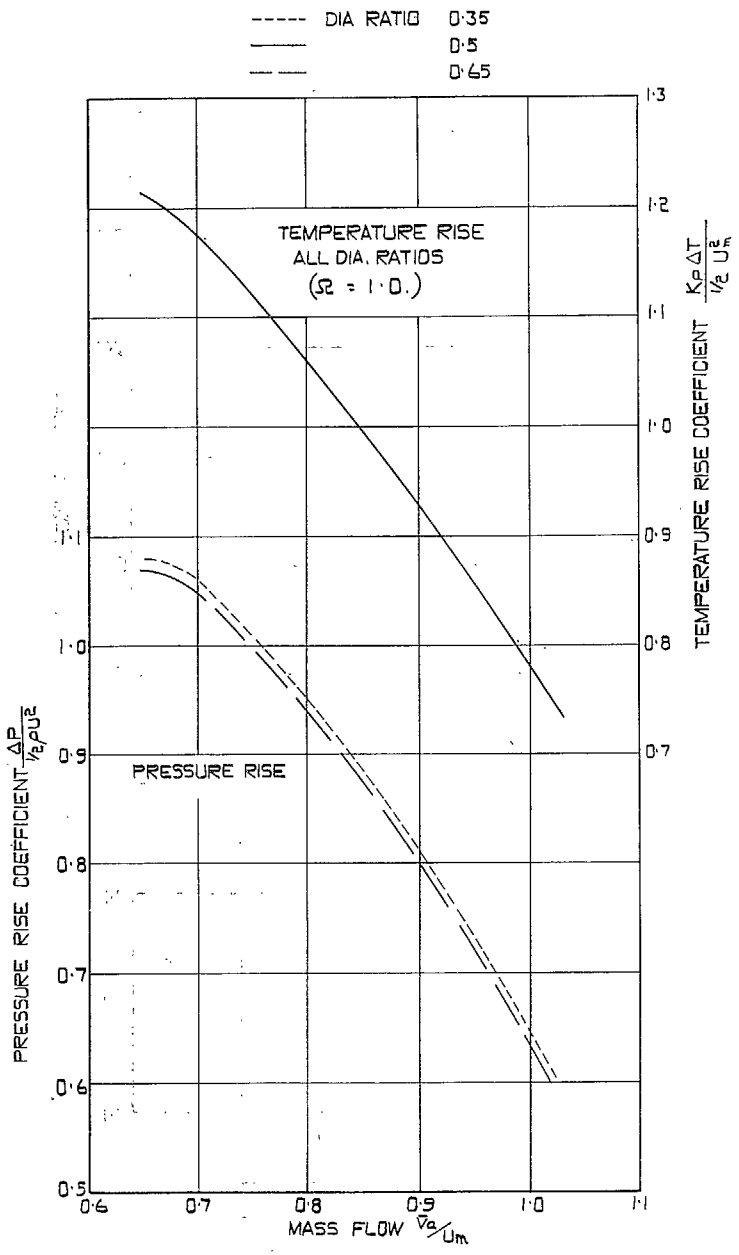

FIG. 6. 'Standard' performance calculation.

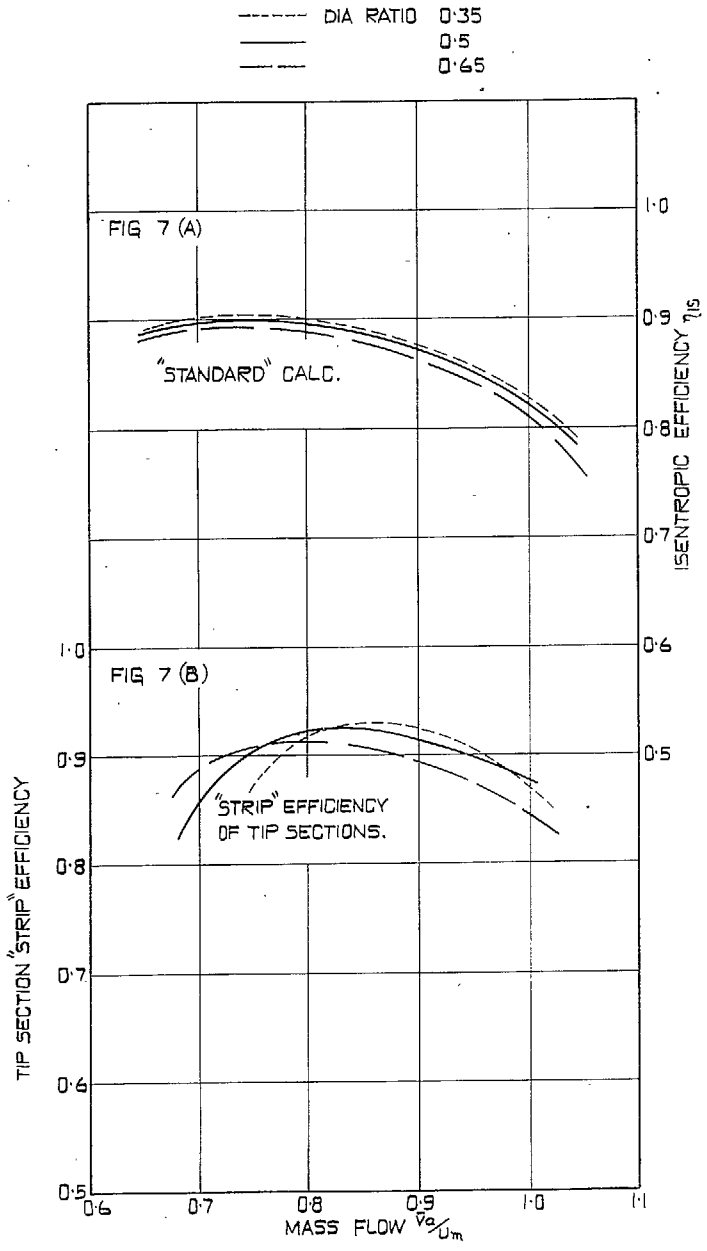

FIGS. 7a and 7b. Theoretical efficiency characteristics.

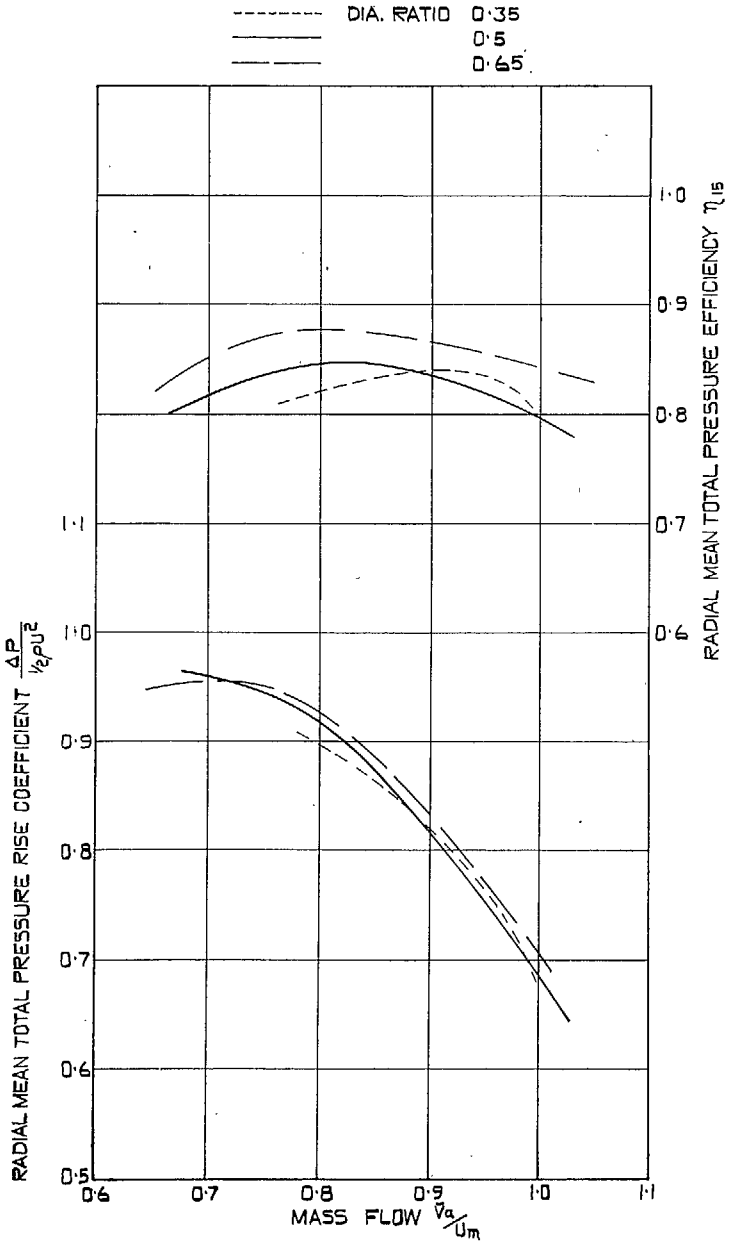

FIG. 8. Experimental characteristics based on radial mean total-pressure rise.

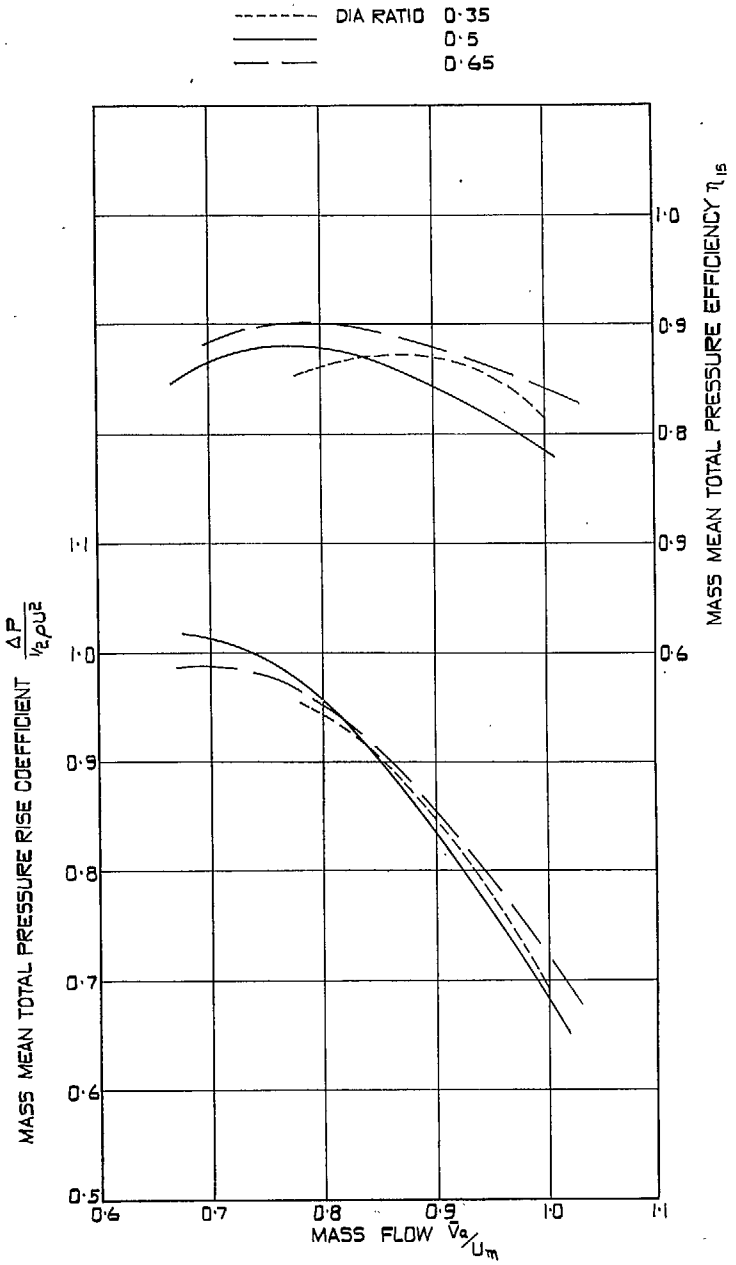

FIG. 9. Experimental characteristics based on mass mean total-pressure rise.

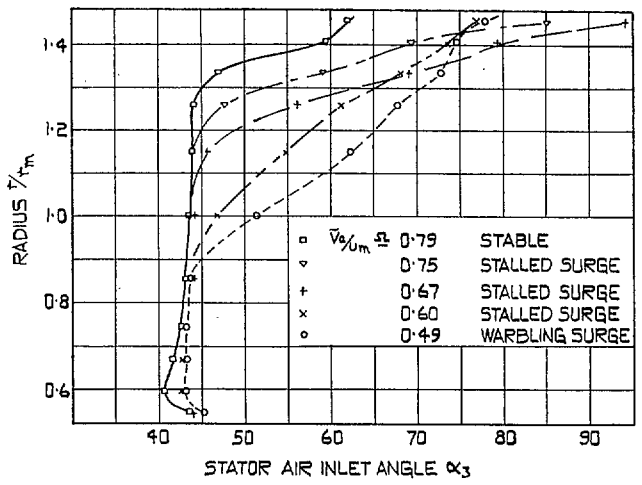

FIG. 10a. Development of air-angle distribution.

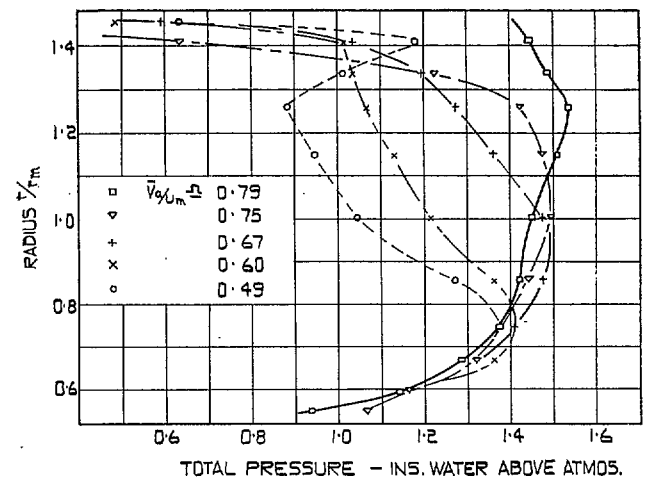

FIG. 10b. Development of total-pressure distribution.

FIGS. 10a and 10b. Development of conditions after rotor compressor 'stalled'. — Diameter ratio 0·35.

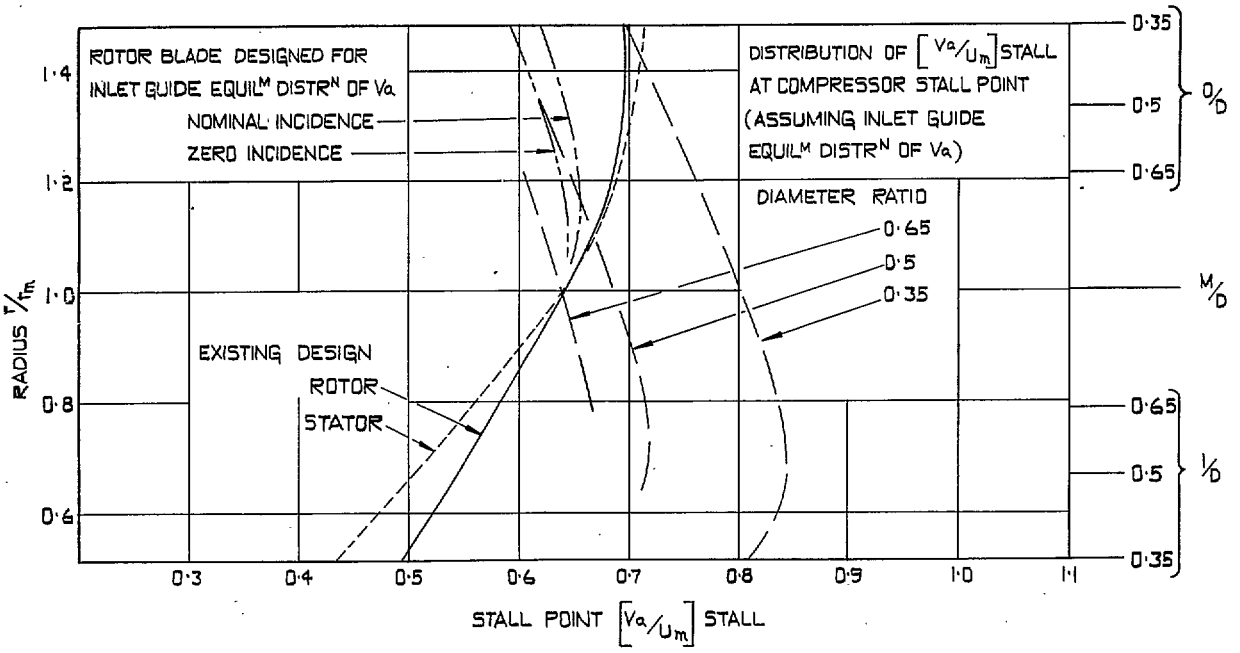

FIG. 11. Blade-section stalling characteristics.

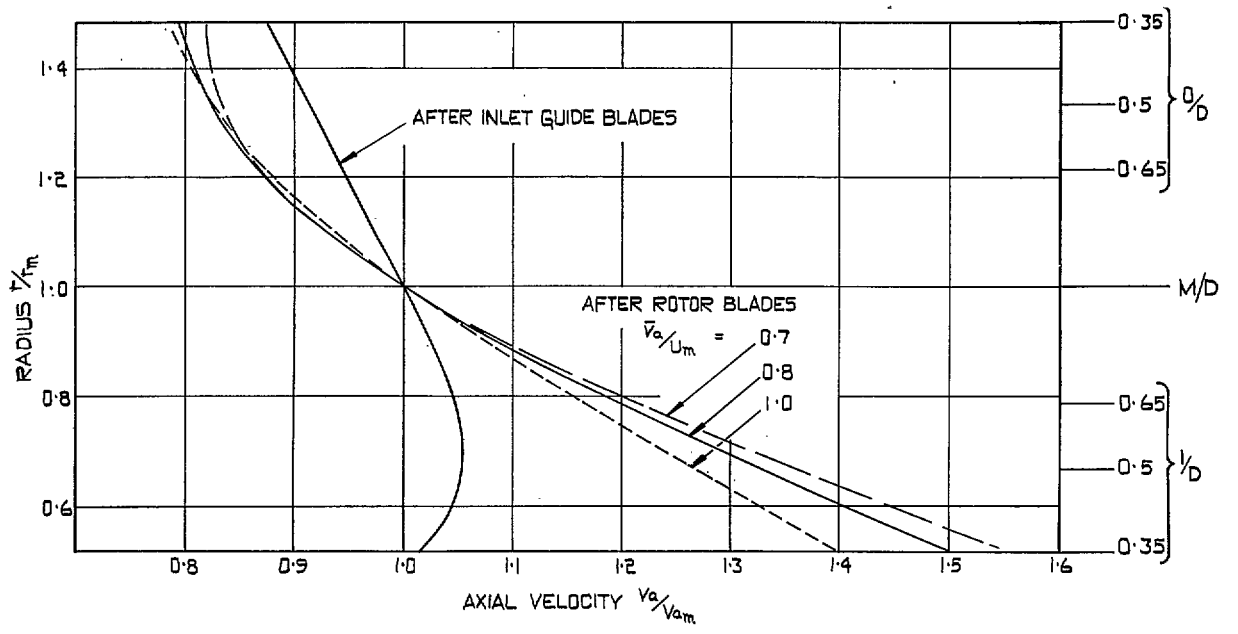

FIG. 12. Radial equilibrium velocity distributions—I.

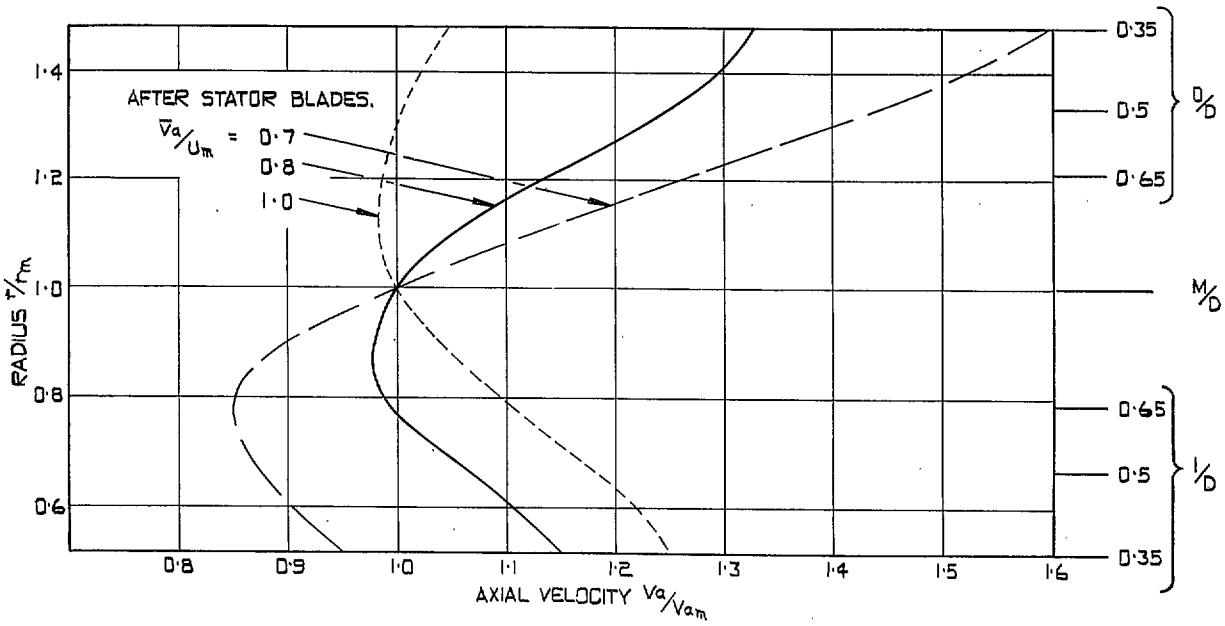

FIG. 13. Radial equilibrium velocity distributions—II.

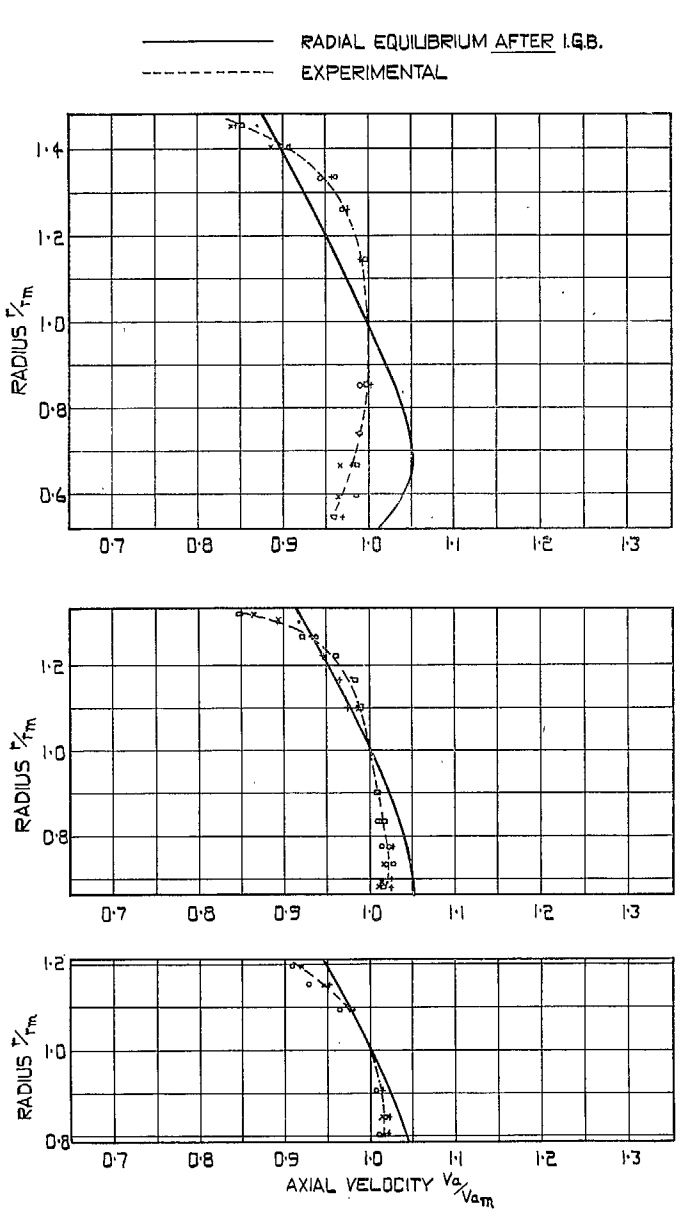

FIG. 14. Axial velocity distributions before inlet guide blades.

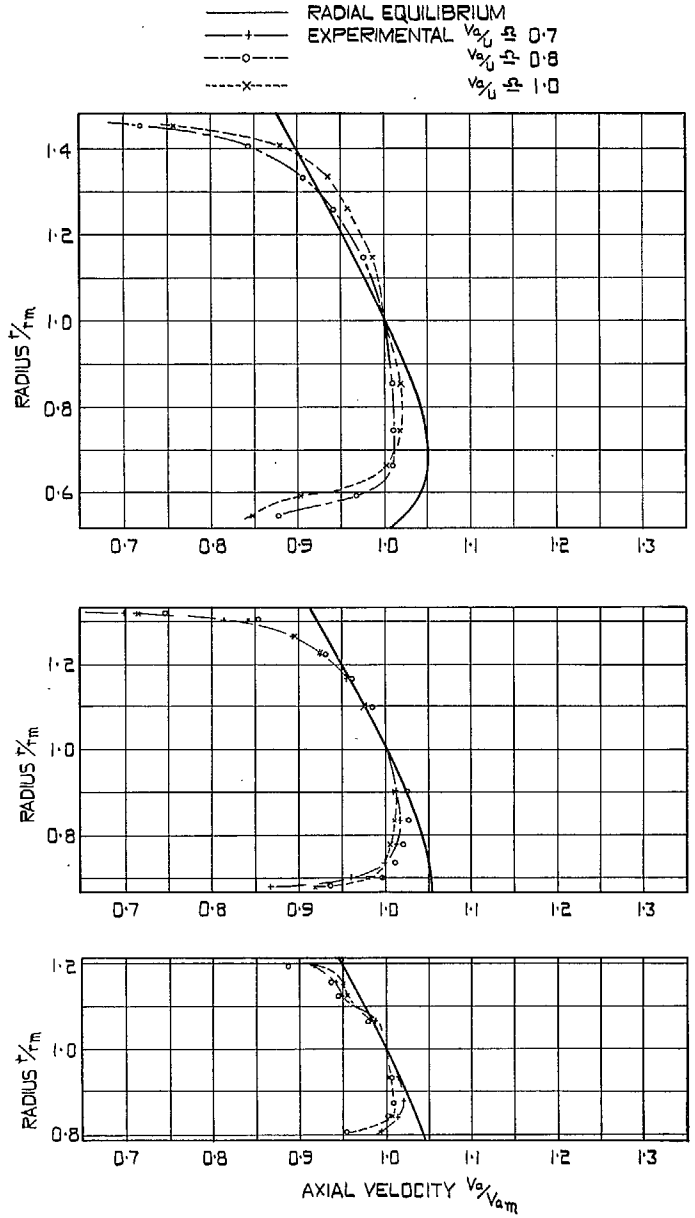

FIG. 15. Axial velocity distributions after inlet guide blades.

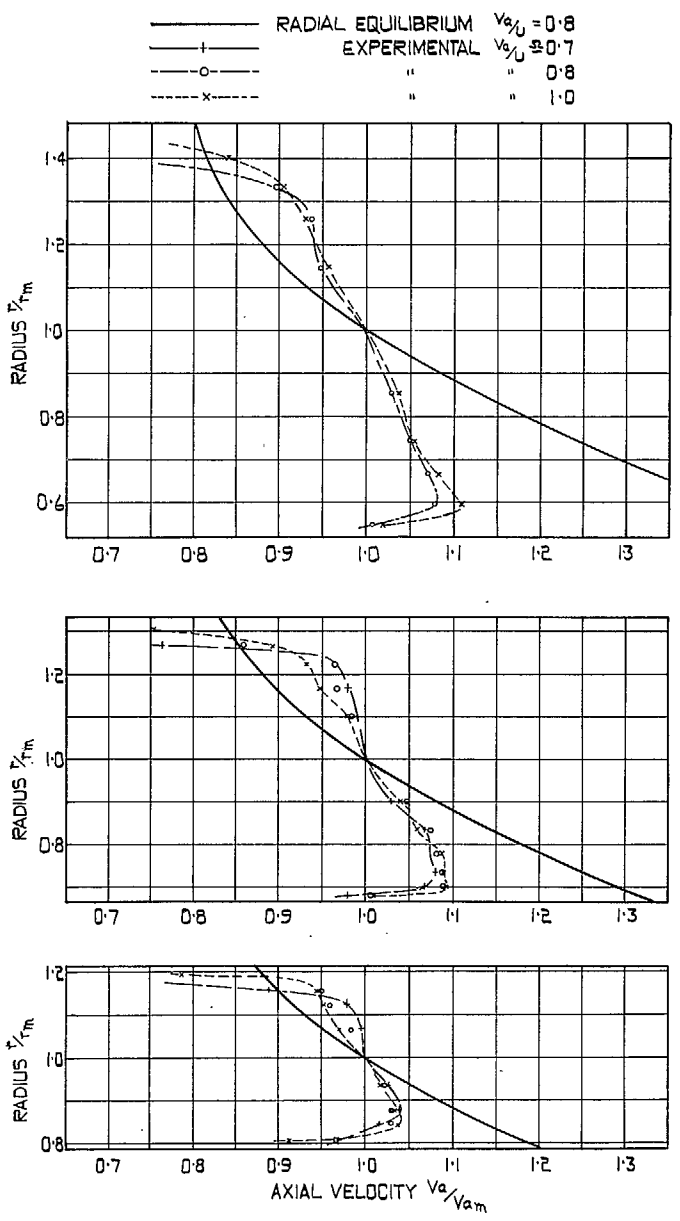

FIG. 16. Axial velocity distributions after rotor blades.

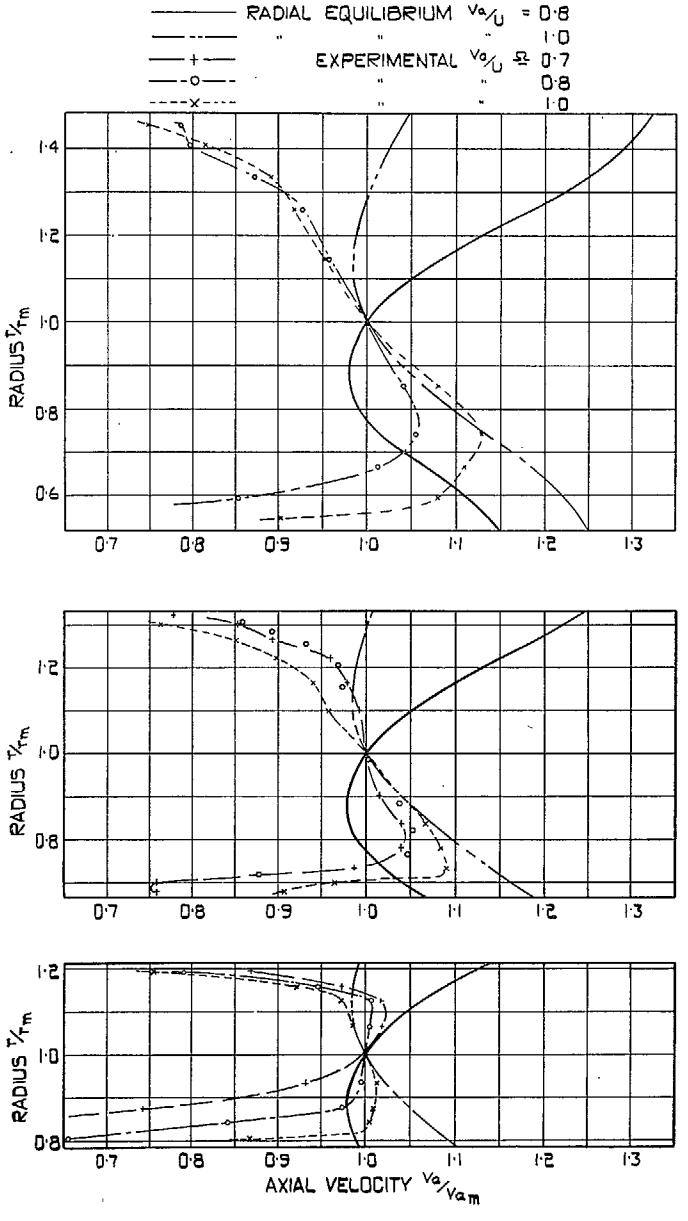

FIG. 17. Axial velocity distributions after stator blades.

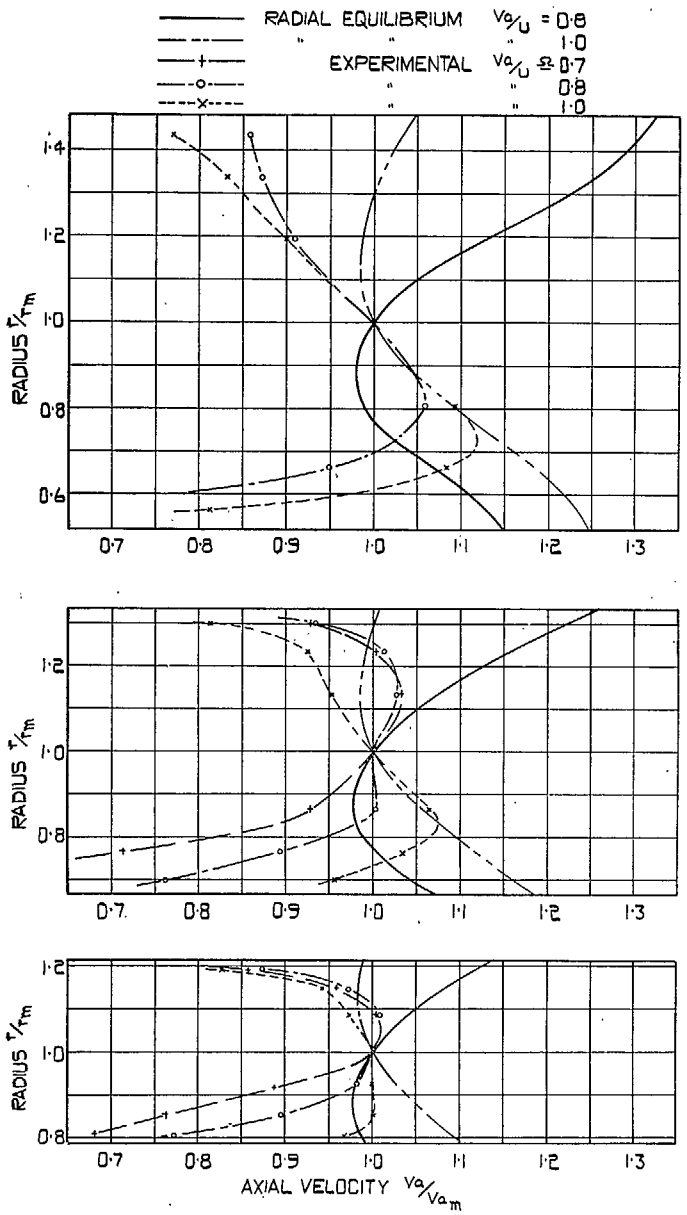

FIG. 18. Axial velocity distributions at pitot comb.

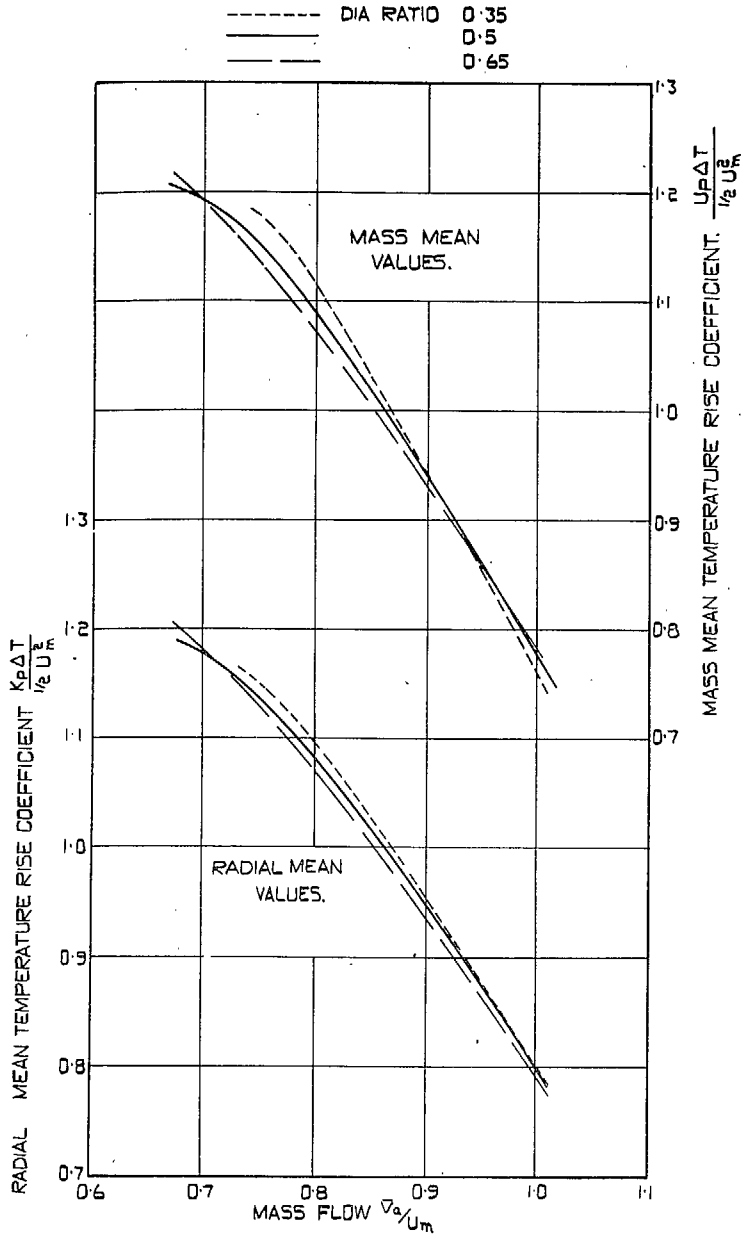

FIG. 19. Theoretical temperature-rise characteristics.

(78426) Wt. 3523/8210 K.7 9/60 Hw.

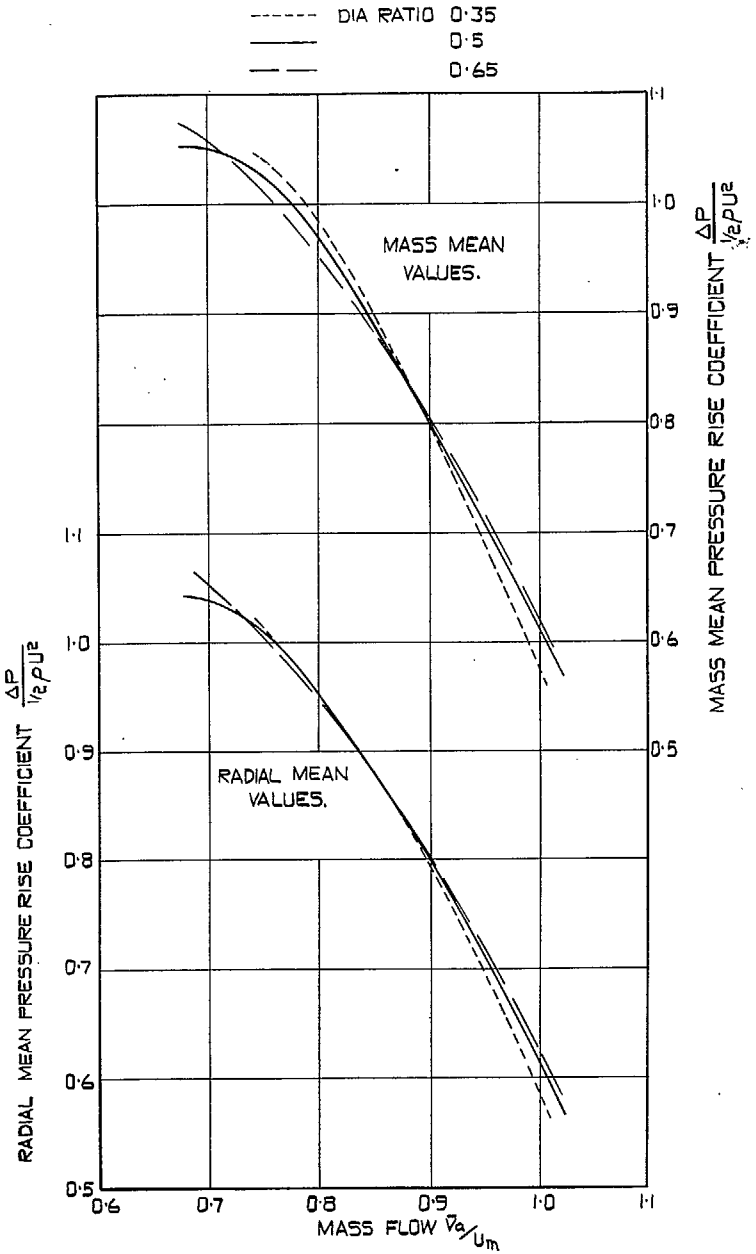

FIG. 20. Theoretical pressure-rise characteristics.

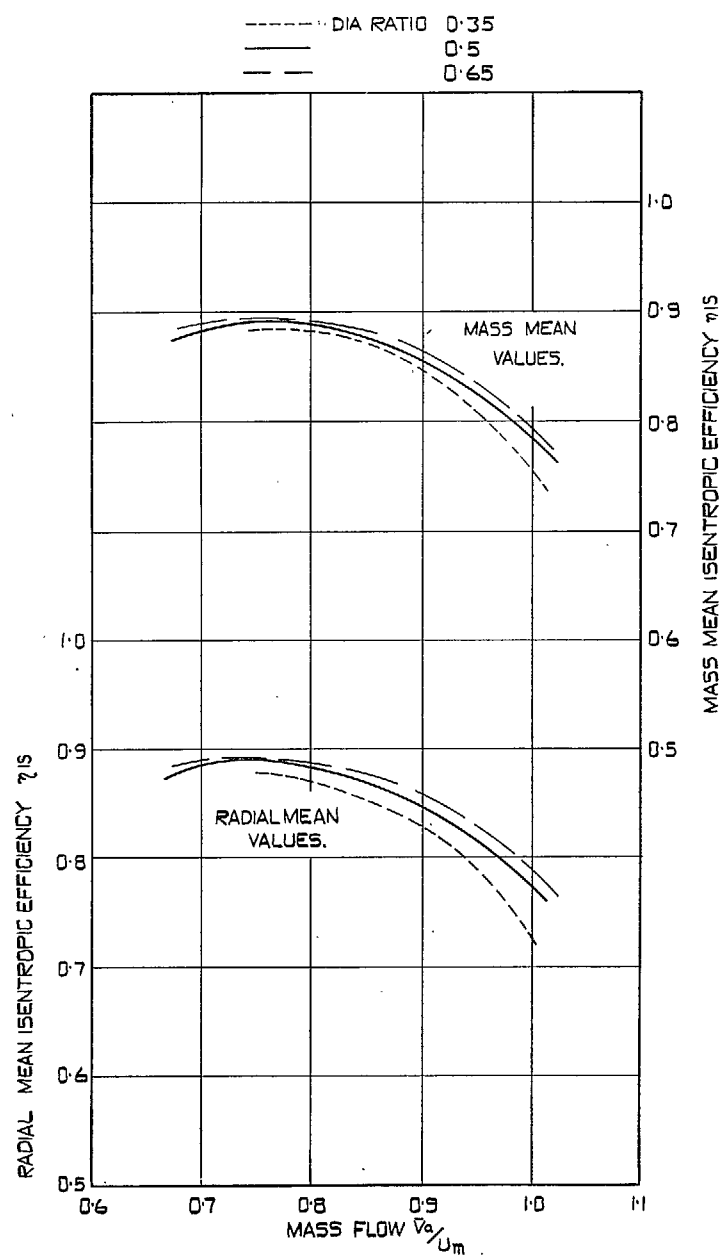

FIG. 21. Theoretical efficiency characteristics.

PRINTED IN ENGLAND

Publications of the Aeronautical Research Council

ANNUAL TECHNICAL REPORTS OF THE AERONAUTICAL RESEARCH COUNCIL (BOUND VOLUMES)

1939 Vol. I. Aerodynamics General, Performance, Airscrews, Engines. 50*s.* (52*s.*)
Vol. II. Stability and Control, Flutter and Vibration, Instruments, Structures, Seaplanes, etc. 63*s.* (65*s.*)

1940 Aero and Hydrodynamics, Aerofoils, Airscrews, Engines, Flutter, Icing, Stability and Control, Structures, and a miscellaneous section. 50*s.* (52*s.*)

1941 Aero and Hydrodynamics, Aerofoils, Airscrews, Engines, Flutter, Stability and Control, Structures. 63*s.* (65*s.* 3*d.*)

1942 Vol. I. Aero and Hydrodynamics, Aerofoils, Airscrews, Engines. 75*s.* (77*s.* 3*d.*)
Vol. II. Noise, Parachutes, Stability and Control, Structures, Vibration, Wind Tunnels. 47*s.* 6*d.* (49*s.* 3*d.*)

1943 Vol. I. Aerodynamics, Aerofoils, Airscrews. 80*s.* (82*s.*)
Vol. II. Engines, Flutter, Materials, Parachutes, Performance, Stability and Control, Structures. 90*s.* (92*s.* 3*d.*)

1944 Vol. I. Aero and Hydrodynamics, Aerofoils, Aircraft, Airscrews, Controls. 84*s.* (86*s.* 6*d.*)
Vol. II. Flutter and Vibration, Materials, Miscellaneous, Navigation, Parachutes, Performance, Plates and Panels, Stability, Structures, Test Equipment, Wind Tunnels. 84*s.* (86*s.* 6*d.*)

1945 Vol. I. Aero and Hydrodynamics, Aerofoils. 130*s.* (133*s.*)
Vol. II. Aircraft, Airscrews, Controls. 130*s.* (133*s.*)
Vol. III. Flutter and Vibration, Instruments, Miscellaneous, Parachutes, Plates and Panels, Propulsion. 130*s.* (132*s.* 9*d.*)
Vol. IV. Stability, Structures, Wind Tunnels, Wind Tunnel Technique. 130*s.* (132*s.* 9*d.*)

1947 Vol. I. Aerodynamics, Aerofoils, Aircraft. 168*s.* (171*s.* 3*d.*)

Annual Reports of the Aeronautical Research Council—

1939–48 3*s.* (3*s.* 5*d.*) 1949–54 5*s.* (5*s.* 5*d.*)

Index to all Reports and Memoranda published in the Annual Technical Reports, and separately—

April, 1950 - - - - R. & M. 2600 6*s.* (6*s.* 2*d.*)

Published Reports and Memoranda of the Aeronautical Research Council—

Between Nos. 2351–2449	R. & M. No. 2450	2*s.* (2*s.* 2*d.*)
Between Nos. 2451–2549	R. & M. No. 2550	2*s.* 6*d.* (2*s.* 8*d.*)
Between Nos. 2551–2649	R. & M. No. 2650	2*s.* 6*d.* (2*s.* 8*d.*)
Between Nos. 2651–2749	R. & M. No. 2750	2*s.* 6*d.* (2*s.* 8*d.*)
Between Nos. 2751–2849	R. & M. No. 2850	2*s.* 6*d.* (2*s.* 8*d.*)
Between Nos. 2851–2949	R. & M. No. 2950	3*s.* (3*s.* 2*d.*)

Prices in brackets include postage

HER MAJESTY'S STATIONERY OFFICE

York House, Kingsway, London W.C.2; 423 Oxford Street, London W.1; 13a Castle Street, Edinburgh 2; 39 King Street, Manchester 2; 2 Edmund Street, Birmingham 3; 109 St. Mary Street, Cardiff; 50 Fairfax Street, Bristol 1; 80 Chichester Street, Belfast 1, *or through any bookseller.*

S.O. Code No. 23-3151